Fuel Processing Technology 277 (2025) 108314

Contents lists available at ScienceDirect

Fuel Processing Technology

journal homepage: www.elsevier.com/locate/fuproc

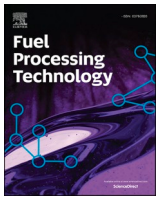

Upcycling Waste to Wealth: CuO-SiO_2/reduced graphene nanocomposite from pomegranate peels for one-pot low-temperature conversion of waste oils into valuable fatty acid monomers

Shahenda Mahran [a,b,*], Maria Centeno [a], Attia Attia [b], Basudeb Saha [c,*]

[a] School of Engineering, London South Bank University, 103 Borough Road, London SE1 0AA, UK
[b] Faculty of Energy and Environmental Engineering, The British University in Egypt, Misr-Ismailia Road, El-Sherouk City, 11837 Cairo, Egypt
[c] School of Engineering, Lancaster University, Lancaster LA1 4YW, UK

ARTICLE INFO

Keywords:
Waste vegetable oil valorisation
Response surface methodology
Green nano-catalyst
Fatty acid-rich monomer
Waste pomegranate peels

ABSTRACT

The utilisation of heterogeneous catalysts in producing fatty acid monomers can minimise the separation cost and hence reduce the price of the fatty acid monomers. This study reports for the first time a novel, environmentally benign, highly active copper oxide-silica oxide/reduced graphene oxide (CuO-SiO_2/RGO), heterogeneous nano-catalyst derived from waste pomegranate peels, for the one-pot, low-temperature synthesis of fatty acid monomers from high-acid-value waste vegetable oil (WVO). The synthesised nano-catalyst was extensively characterised using XRD, FT-IR, TEM, SEM, EDX and TGA-DTA. Further, it was utilised to synthesise fatty acid-rich oleic phenoxypropyl acrylate (OPA) monomer from high acid value WVO via a single-step reaction. The process parameters for the synthesis of OPA monomer using CuO-SiO_2/RGO catalyst have been optimised using response surface methodology (RSM) and found to be 8.5:1 reactant molar ratio, 3.5 % (*w*/w) catalyst loading, 54 °C temperature, and 9.5 h reaction time, where the highest OPA monomer yield was 95.73 % under optimum conditions. The CuO-SiO_2/RGO exhibited stable catalytic performance after regeneration with an OPA yield of 93.1 ± 0.37 % after five consecutive runs. The plausible reaction mechanism unveiled that the direct synthesis of OPA monomer from high acid value WVO occurred through both transesterification and esterification reactions simultaneously on the surface of CuO and SiO2 catalyst supported on RGO sheets. The adaptation of waste pomegranate peels into a high-value CuO-SiO_2/RGO nano-catalyst offers a new direction for clean, one-pot and low-temperature production of sustainable fatty acid monomers from high-acid-value WVO.

1. Introduction

Waste vegetable oils (WVOs) and their derived fatty acids are crucial sustainable materials for the synthesis of high-value chemicals due to their abundance, low cost, and potential to diminish environmental waste [1]. The rapid increase of global production of WVO, exceeding 190 million metric tons per year, including about 1 million tons per year from the European Union (EU), provides an eco-friendly alternative to fossil-based resources [2]. According to Mannu et al. [3], millions of dollars are spent on WVO processing and recycling annually to be used as raw material for different applications. Recently, the literature has reported the application of renewable resources for the synthesis of biopolymers for different industrial applications [4–13]. The unsaturated nature of vegetable oils favours functionalisation reaction, which improves the hydrophilic properties of vegetable oil-derived materials despite the existence of long fatty acid alkyl chains [14]. The literature reported the utilisation of edible vegetable oils as a sustainable platform for the synthesis of fatty acid derivatives and monomers, owing to their worldwide availability, nontoxicity, and low cost [1,15,16].For the synthesis of fatty acid monomers, the catalyst should not only enhance the yield of the synthesised bio-monomer but also achieve the required conditions for a cleaner and sustainable chemical process [17]. Homogeneous catalysts are the most applied catalysts for the synthesis of fatty acid-based monomers [18]. Yuan et al. [14] employed sodium methoxide catalyst in the transesterification reaction between vegetable oil and amino alcohols for the synthesis of N-hydroxyalkyl fatty amides, which are further converted into fatty acid monomers. Homogeneous catalysis has also been utilised for the esterification reaction of fatty

* Corresponding authors.
E-mail addresses: Shahenda.Mahran@bue.edu.eg (S. Mahran), b.saha@lancaster.ac.uk (B. Saha).

https://doi.org/10.1016/j.fuproc.2025.108314
Received 7 June 2025; Received in revised form 5 August 2025; Accepted 18 August 2025
Available online 27 August 2025

acids and methacrylate to synthesise fatty acid derivatives [19]. Mhadeshwar et al. [20] synthesised ricinoleic acid monomer through the esterification of ricinoleic acid with 2-hydroxyethyl methacrylate using butylstannoic acid as a catalyst. Machado et al. [21] reported the synthesis of diene monomer via esterification of 10-undecenoic acid and isosorbide. These monomers, practically with methyl (or ethyl) 10-undecenoate, were synthesised using 4,4-dimethylaminopyridine [22]; 1,1-carbonyl diimidazole [23], NaOMe or NEt_3 [24] and p-toluene sulfonic acid or scandium(III) triflate $Sc\text{-}(CF_3SO_3)_3$ [25]. Other researchers reported the synthesis of fatty acid-based monomers by reacting acid chloride with diols using the NEt_3 catalyst [26,27]. The literature also reported the synthesis of fatty acid-based monomers by reacting acid chloride with diols using NEt_3 catalyst [26,27]. Similarly, the literature reported the synthesis of oleic estolides under the catalysis of sulphuric acid (H_2SO_4), perchloric acid ($HClO_4$), *p*-toluenesulfonic acid, or montmorillonite [28–31]. Despite the application of homogeneous catalysts in the synthesis of the fatty acid monomers produced a relatively high fatty acid monomer yield that ranges from 86 % to 91 % at mild temperatures up to 60 °C they have limitations that involve the difficulty of catalyst separation, catalyst reusability is not possible along with the production of a large amount of wastewater during the purification process that subsequently increases the manufacturing cost of materials and raises many environmental concerns [32–34].

To overcome the shortcomings, the utilisation of heterogeneous catalysts is favoured as it is easily regenerated, recycled and minimises the separation and purification cost that increases its commercial production [35–38]. Recently, the literature reported the utilisation of different heterogeneous catalysts for the synthesis of epoxy fatty acid derivatives from vegetable oil. These heterogeneous catalysts include acidic ion exchange resins (AIERs) [39–43] and metal heterogeneous catalysts [44–48] in the presence of oxidants, mostly hydrogen peroxide and percarboxylic acid as an oxygen carrier [39–43]. Other researchers also reported the utilisation of heterogeneous catalysts for the synthesis of fatty acid monomers. Moreno et al. [12,49] have reported the application of Cr III and zinc-based catalysts for the synthesis of methacrylated linoleic acid monomer through the esterification of linoleic acid with glycidyl methacrylate. However, catalyst reusability has not been reported. Several heterogeneous catalysts have also been recently reported for the conversion of fatty acids to α-olefin fatty acid vinyl monomers, which include silver nitrate [50], Pd on non-oxidised CNF [51,52], Pd/Al_2O_3 [53], $ZnCl_2$ [54,55], Pd/C [56–58], Pd on oxidised CNF [51,52,59], and Palladium [79]. These studies reported low selectivity of less than 60 % of the resultant fatty acid monomers due to the presence of ketones, saturated hydrocarbons, and cracking products byproducts [52,59]. Furthermore, these catalysts are operated at extremely high reaction temperatures and long reaction time ranges from 200 to 350 °C and 24 h, respectively, and prepared from high-cost commercial materials, which limits the commercial application of these catalysts in fatty acid monomer production. Therefore, it is essential to design a novel green catalytic process with high performance for the synthesis of fatty acid vinyl monomers with a high yield that could operate at lower reaction temperatures and less reaction time. According to the literature, no previous studies have been reported so far approaching the synthesis of green, heterogeneous, nano-catalysts for the synthesis of fatty acid-rich monomers. Furthermore, the utilisation of green heterogeneous nano-catalysts in the synthesis of fatty acid monomers from WVO has not been reported.

The valorisation of agro-industrial waste, such as pomegranate peels, into a cost-effective catalyst for the synthesis of fatty acid monomers could be a smart alternative to high-cost catalytic materials. Pomegranate peels are rich in phenolic compounds characterised by a high antioxidant activity, involving flavonoids such as phenolic compounds and tannins such as punicalagin and gallic acid [60,61]. which can behave as a reducing agent for the synthesis of nanoparticles [62,63]. Pomegranate peels account for up to 55% of the pomegranate weight, and it is disposed contempt a large quantity of phenolic compounds [62–64]. The global production of pomegranates is 3 million tons annually, and 1.62 million tons are waste, including peels. This waste has a hazardous impact on the environment and reduces economic production as they are disposed of. Using this waste in the synthesis of nano-catalysts promotes their circular economy and diminishes environmental pollution. Current studies are investigating the innovative utilisation of phenolic-containing plant extracts for the green synthesis of nanomaterials. Although the synthesis of polyphenol-derived single nanoparticles [65–67] or binary systems [68,69] and graphene oxide-based materials [70,71] with a single metal oxide has been recently reported in the literature, the utilisation of PPE as the sole reducing and stabilising agent for the synthesis of a hybrid, multifunctional $CuO–SiO_2$/RGO nanocomposite specifically tailored for one-pot, low-temperature fatty acid monomer production remains unexplored. Recently, some researchers have reported on the utilisation of nanoparticles as catalysts for transesterification reactions due to their high surface area and nanoparticle size. Nano-catalysts can accelerate the rate of reaction owing to a high number of molecules consuming minimal energy essential for the reaction to happen [17,33]. From various materials that can be utilised to synthesise nanocomposites, graphene-based materials provide unique properties as it is inert in basic and acidic media and easy to change their chemical properties. Moreover, it has a high surface area and high efficiency as a charge carrier. [33] and high interfacial interaction with metal nanoparticles, with ease of movement of charge within the surface, leading to synergistic influence, which improves the catalytic performance of the composite [17]. Various researchers presented the utilisation of graphene-based materials as a catalyst for biofuel production and dimethyl carbonate; however, no studies have been reported on their potential in the synthesis of fatty acid monomers.

In our recently published work, we reported the synthesis of fatty acid-rich OPA monomer using 4-(dimethylamino)pyridine (DMAP) homogenous catalyst through the transesterification of fatty acid methyl ester (FAME) via multi-stage reaction [1]. The usage of DMAP homogenous catalyst increased the separation cost and environmental concerns associated with the production of wastewater during the purification process of synthesised OPA monomer. Also, catalyst separation and reusability were not applicable [72]. In this context, the current research reports the valorisation of waste pomegranate peels into a novel, green, cost-effective $CuO\text{-}SiO_2$/RGO nanocomposite heterogeneous catalyst tailored for a cleaner, direct and low temperature transformation of high acid value WVO into valuable fatty acid-rich monomer via a single step transesterification reaction. The synthesised nano-catalyst has been characterised by XRD, FT-IR, SEM, EDX, TEM and TGA-DTA. The RSM approach has been used to optimise synthetic parameters for the OPA monomer preparation by varying four controllable variables (reactant molar ratio, catalyst loading, reaction temperature, and reaction time) at three levels. The values of the predicted response (OPA monomer yield) using RSM were compared with the experimental yield of OPA monomer. Furthermore, the relationship between the yield of OPA monomer and the synthesis parameters was also studied based on the experimental results. The regression analysis has been utilised to develop the validated model to conclude the optimum reaction conditions for maximising OPA yield. Further, the chemical structure of the OPA monomer has been confirmed. According to the literature, this is the first study of the synthesis of a competitive, green, heterogeneous nano-catalyst tailored for a cleaner and direct transformation of a high acid value WVO into a valuable fatty acid-rich monomer using a single-step reaction and low reaction conditions. The green $CuO\text{-}SiO_2$/RGO PPE-derived nanocomposite developed in this research is uniquely designed to catalyse both esterification and transesterification reactions simultaneously, for one-pot, low temperature OPA monomer synthesis from high acid the approach not previously reported. In addition to the utilisation of systematic optimisation of response surface methodology (RSM) to maximise OPA monomer yield under mild reaction conditions. Therefore, the integration of waste valorisation, green heterogenous

nano-catalyst and statistical process optimisation in this research offers an innovative, cleaner, cost-effective approach for the synthesis of fatty acid-rich polymer precursors from high acid-value WVO using a single-step reaction as an alternative to existing multistage approaches of applying homogeneous catalysts.

2. Experimental section

2.1. Materials

WVO feedstock was collected from restaurants in Egypt (TAN evaluated using ASTM D-974 method is 10 mg KOH g^{-1}, density evaluated using ASTM D-4052 is 0.93 g/cm^3); Pomegranate peels were collected from juice stores in Egypt, natural graphite powder, potassium permanganate ($KMnO_4$), sulphuric acid (H_2SO_4), hydrogen peroxide (H_2O_2), hydrochloric acid (HCl), *p*-cymene (99 %), 2-hydroxy-3-phenoxypropyl acrylate (HPA), sodium metasilicate (Na_2SiO_3), copper chloride ($CuCl_2$), methyl hydroquinone (MEHQ), dimethyl sulfoxide-d_6 (99.9 atom %D) were supplied by Sigma-Aldrich.

2.2. Synthesis of CuO-SiO_2/RGO nanocomposite catalyst

The synthesis of CuO-SiO_2/RGO nanocomposite was performed as indicated in Fig. 1. Initially, Graphene oxide (GO) was synthesised according to Hummer's method with minor modifications [17,73,74]. In a 500 mL conical flask, 2 g of graphite powder was dissolved in 46 mL concentrated H_2SO_4 and stirred. 6 g of $KMnO_4$ was added dropwise. The mixture was stirred for 2 h at a temperature of −5 °C. The mixture was then heated to 40 °C with stirring for 12 h. Further, 92 mL of deionised water is added to the mixture under continuous stirring. Thereafter, 35 % H_2O_2 was added dropwise, followed by 5 % HCl solution. The reaction solution was then washed with deionised water to remove unreacted salts and acids. Further, pomegranate peel extract (PPE) was prepared by dissolving 16 g of pomegranate peel powder in 200 mL of deionised water and heating the mixture to 40 °C for 1 h. The solution was then filtered, and the PPE was kept at 4 °C. To prepare CuO-SiO_2/RGO, 400 mg of GO powder was dispersed in 40 mL of deionised water by sonication. The GO dispersion was transferred to a round flask, then 1 g of $CuCl_2$ and 2.5 g of Na_2SiO_3 were added dropwise to the GO dispersion. The reaction mixture was then refluxed at 90 °C with a100 mg of PPE solution (0.4 g mL^{-1}) with stirring for 8 h. The mixture was then cooled to 25 °C, and the precipitate of the nanocomposite was collected by filtration. PPE solution concentration ranging from 0.21 g mL^{-1} to 0.43 g mL^{-1} was selected to evaluate its effect on the catalyst's chemical structure, size and morphology. This range was selected based on preliminary experiments, indicated that higher PPE concentration above 0.43 g mL^{-1} resulted in a significant increase in the reaction medium viscosity, which diminished mixing and diffusion within the reaction medium, resulting in ineffective mass transfer and incomplete reduction of metal ions. The synthesis protocol of the CuO-SiO_2/RGO nanocomposite catalyst is shown in Fig. 1.

2.3. Synthesis of fatty acid-rich oleic phenoxypropyl acrylate monomer (OPA)

Both transesterification and esterification reactions simultaneously occurred between 2-hydroxy-3-phenoxypropyl acrylate (HPA) and both triglycerides and fatty acids that exist in WVO, respectively. SiO_2 works as a catalyst in the esterification reaction[75], and CuO contributes to the transesterification reaction [76]. In a 250 mL jacketed reactor equipped with a thermometer and mechanical stirrer, 90 mL of p-cymene was charged into the reactor as a solvent, followed by the designed amounts of HPA and WVO (according to the specified molar ratio of each run). The designed weight of the synthesised catalyst was dispersed in *p*-cymene and added to the reaction mixture dropwise over 20 min, then 1.2 % (*w*/w) methylhydroquinone was added to the reaction mixture.

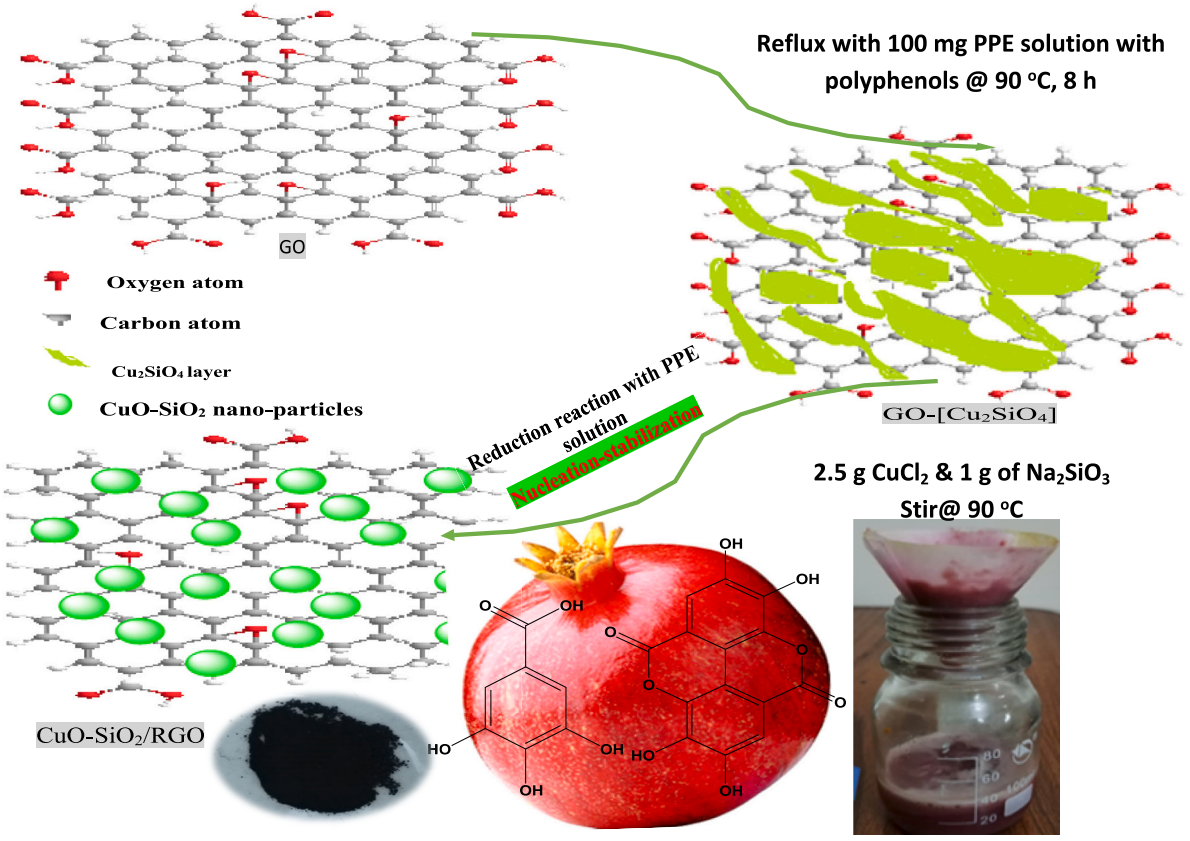

Fig. 1. Synthesis protocol of CuO-SiO_2/RGO nanocomposite catalyst.

The reaction mixture was then stirred at different temperatures for the specified reaction durations. After the designed reaction time, the mixture was centrifuged, and the synthesised product was separated from the produced glycerol and water during esterification and trans-esterification reactions. The catalyst was separated by centrifuge and denoted as a fresh catalyst, and then the reusability studies of the CuO-SiO_2/RGO catalyst were conducted. The catalyst was reused for 5 cycles of reactions without any treatment. Regeneration of the catalyst was performed after the accomplishment of the catalyst reusability for 5 cycles. The catalyst was separated after the cycle and regenerated before being reused for another 5 runs. After the reusability of the catalyst in 5 consecutive cycles, the catalyst was regenerated by washing with methanol, followed by drying in an oven at 80 °C for 1 h. This was followed by calcination of the catalyst in a vertical furnace in the presence of argon at 300 °C using a ramp rate of 10 °C/min for 3 h to be re-used for the next cycles at the same reaction conditions. The isolated OPA monomer was rinsed with methanol and dried with magnesium sulfate under vacuum. Further, the OPA monomer yield was calculated based on the ratio of the mass of the product to the reactants [77].

2.4. Characterisation techniques

The gas chromatography–mass spectrometry (GC–MS) analysis and physicochemical properties of WVO feedstock were discussed in detail elsewhere [72]. The phase structure of the prepared nanocomposite catalyst was analysed by X-ray diffractometer (Rigaku Miniflex, Japan) using CuKa radiation at 30 KV in the 2θ range of 10-80°. The identification of functional groups in the synthesised nanocomposite catalyst was performed using an FT-IR spectrometer (Shimadzu FTIR-8400). The morphology and elemental composition of the nanocomposite catalyst were investigated by Scanning Electron Microscope (SEM; Hitachi S-4800 II Model), which was connected with Energy Dispersive X-ray (EDX) spectroscopy. The structural and morphological properties of the catalyst were evaluated using Transmission Electron Microscopy (TEM) images using (JEM-2100F, 200 kV). The ^{1}H NMR of the synthesised monomer was performed by a Bruker Avance 400 spectrometer, Rheinstetten, Germany. Thermogravimetric analysis was performed using a Shimadzu TGA-50 thermogravimetric analyser.

2.5. Experimental design

A three-level-four-factor, BBD was applied in this optimisation study. The influence of four independent variables on the OPA monomer yield was investigated. The independent variables were identified as molar ratio of HPA:WVO (A), catalyst loading (B), temperature (C) and time (D) to optimise the process parameters for the synthesis of the OPA monomer. The coded and actual levels of the four independent variables are indicated in Table 1. The values of the four variables were defined based on preliminary experiments. The WVO:HPA molar ratio (2:1–10:1) was selected to cover stoichiometric and excess reactant conditions. Catalyst loading (0.5–3.5 wt%) is the typical range to avoid mass-transfer limitations. The temperature range (40–130 °C) involves both mild to moderate reaction conditions, ensuring no HPA degradation, whereas the reaction time (2–15 h) was selected to allow evaluation of kinetic and equilibrium phases. BBD has been utilised to design a set of experiments for evaluating the relation between process variables and reaction response. Twenty-nine experiments have been generated using the defined variables and levels. Design Expert 11 software (Stat-Ease Inc., Minneapolis, MN, USA) was utilised to design experimental runs. Table 2 indicates the experimental design along with the predicted response of OPA monomer yield.

Table 1
Experimental design variables and their coded levels.

Factor	Code	Levels		
		-1	0	+1
WVO: HPA (molar ratio)	A	2	2.66	10.00
Catalyst loading (%) (w/w)	B	0.5	1.5	3.5
Reaction temperature (°C)	C	40	85	130
Reaction time (h)	D	2	6	15

2.6. Statistical analysis

Regression analysis was completed by applying a quadratic polynomial equation to state the model as indicated in Eq. (10). Where: Y, the dependent response; β_0, coefficient constant; β_i, β_{ii}, β_{ij}, intercept coefficient of linear, quadratic, interactive terms respectively, X_i, X_j, model-independent variables ($i \neq j$).

$$Y = b_o + \sum_{i=1}^{n} b_i x_i + \sum_{i=1}^{n} b_{ii} x_i^2 + \sum_{i=1}^{n-1} \sum_{j>1}^{n} b_{ij} x_i x_j + \varepsilon \quad (10)$$

The adequacy of the model was evaluated using ANOVA by calculating Fisher's F-test value at a 95 % confidence level. The statistical significance of model variables was expressed by *p*-value, as the variable is significant when the p-value is less than 0.05. Moreover, Lack-of-fit analysis is one of the crucial analyses by ANOVA, which evaluates the failure of the developed model to represent the actual experimental results. The accuracy of the generated model to fit the experimental data can be determined from the significance of the regression analysis and the insignificance of the lack of fit value [78]. The lack of fit and the value of pure error indicated in Table 3 prove the good reproducibility of the experimental results. The predicted OPA yield is summarised in Table 2, which was estimated using the developed model.

3. Results and discussion

The characterisation results of the synthesised CuO-SiO_2/RGO nanocomposite catalyst, along with the OPA fatty acid monomer, have been discussed in this section. Furthermore, the results of the RSM optimisation of the synthesis parameters of the OPA fatty acid monomer using CuO-SiO_2/RGO nanocomposite catalyst have been presented in detail.

3.1. Characterisation of CuO-SiO_2/RGO nanocomposite catalyst

3.1.1. X-ray diffraction of synthesised CuO-SiO_2/RGO nanocomposite catalyst

The XRD pattern of GO, the control nanocomposite prepared without PPE and CuO-SiO_2/RGO nanocomposites prepared with different PPE solution concentrations ranging from 0.21 g mL^{-1} to 0.43 g mL^{-1} are shown in Fig. 2(a). The XRD pattern of GO indicates a diffraction peak at ~10.48 corresponding to (002) of GO, revealing the successful oxidation of graphite powder to GO [79]. The diffraction peaks observed at 2θ =32.5, 35.45, 54.1, 58.2, 62.50, 67.1, 72.04, and 75.8 corresponds to (110), (11−1), (020), (202), (113), (022), (311) and (004), respectively attributed to CuO matched with JCPDS file (48–1548) as reported in other studies [80]. The XRD pattern also demonstrates a broad peak at 23° due to the amorphous phase of SiO_2. It can be observed that all the diffracted peaks are intensified with the increase in PPE concentration, which confirms the crystallinity of the nanocomposite. The average particle size of CuO-SiO_2/RGO prepared with 0.43 g mL^{-1} PPE solution was evaluated from the diffraction peak with the highest intensity (2θ = 32.51°) by applying the Scherrer equation and determined to be 7 nm. It was observed that with the increase of the applied PPE concentration, the diffraction peaks showed higher intensity, and the crystallite phase became more regular. The XRD pattern mainly demonstrates the existence of a CuO crystalline phase with improved crystallinity and size as the PPE solution concentration increased to 0.43 g mL^{-1}. The increase of PPE concentration decreased the crystallite size of the synthesised catalyst from 35 nm to 7 nm, which can be attributed to the shielding

Table 2
Experimental design matrix with the actual and predicted yield of OPA monomer.

Entry	WVO:HPA (molar ratio)(A)	Catalyst loading (%)(B)	Reaction temperature, (°C)(C)	Reaction time (h) (D)	Isolated OPA yield%	Predicted OPA yield%	Residuals
1	10	2	85	1	30.2	29.29	0.91
2	6	2	130	1	20.7	20.00	0.7
3	6	0.5	40	8	23.5	28.79	−5.29
4	10	2	85	15	79.1	75.96	3.14
5	6	2	85	8	86.8	84.00	2.8
6	6	3.5	85	15	75.5	77.21	−1.71
7	6	0.5	85	15	36.1	39.04	−2.94
8	6	0.5	130	8	39.1	35.13	3.97
9	2	3.5	85	8	30.3	33.17	−2.87
10	6	2	85	8	84.5	84.00	0.5
11	10	2	130	8	70.6	76.04	−5.44
12	6	3.5	130	8	86.4	76.29	10.11
13	2	2	40	8	20.2	17.54	2.66
14	6	0.5	85	1	30.2	31.37	−1.17
15	6	2	130	15	70.8	70.67	0.13
16	10	2	40	8	26.2	22.71	3.49
17	6	2	85	8	85.3	84.00	1.3
18	2	2	130	8	15.2	21.88	−6.68
19	2	2	85	1	20.1	19.13	0.97
20	6	3.5	40	8	25.2	24.96	0.24
21	2	0.5	85	8	37.8	33.50	4.3
22	6	2	40	1	15.2	14.67	0.53
23	10	0.5	85	8	47.8	44.17	3.63
24	10	3.5	85	8	78.1	81.83	−3.73
25	6	2	85	8	85.2	84.00	1.2
26	6	2	40	15	18.2	18.33	−0.13
27	2	2	85	15	30.8	26.79	4.01
28	6	2	85	8	80.5	84.00	−3.5
29	6	3.5	85	1	30.1	30.54	−0.44

Table 3
Analysis of variance for yield of OPA monomer model.

Source	Sum of Squares	df	Mean Square	F-value	p-value	Significance
Model	20,172.51	14	1440.89	57.93	< 0.0001	HS
A-HPA:WVO	2640.33	1	2640.33	106.14	< 0.0001	HS
B-Catalyst loading	1045.33	1	1045.33	42.02	< 0.0001	HS
C-Temperature	2494.08	1	2494.08	100.26	< 0.0001	HS
D-Time	2214.08	1	2214.08	89.01	< 0.0001	HS
AB	361	1	361	14.51	0.0065	S
AC	600.25	1	600.25	24.13	0.0002	S
AD	380.25	1	380.25	15.29	0.0013	S
BC	506.25	1	506.25	20.35	0.0004	S
BD	380.25	1	380.25	15.29	0.0003	S
CD	552.25	1	552.25	22.2	0.0003	S
A^2	2940.55	1	2940.55	118.21	< 0.0001	HS
B^2	1371.63	1	1371.63	55.14	< 0.0001	HS
C^2	5146.13	1	5146.13	206.88	< 0.0001	HS
D^2	4027.07	1	4027.07	161.89	< 0.0001	HS
Residual	348.25	14	24.88			
Lack of Fit	326.25	10	32.63	5.93	0.0558	NS
Pure Error	22	4	5.5			
Cor Total	20,520.76	28				

[a] HS: Highly Significant, S: Significant and NS: Not Significant.

effect of PPE that modifies the size and shape of the particles to a nanosized range where polyphenols of PPE behave as a reducing agent. The decrease of the nano-particle size with the increase of PPE concentration can be attributed to an improved reduction reaction rate along with accelerated reaction kinetics with the increase of polyphenols concentration contained in higher concentrations of PPE, which results in fast nucleation of the formed nanoparticles. The accelerated nucleation owing to the higher concentration of polyphenols results in a rapid decrease in the size of the formed nanoparticles. The behaviour that can be justified by fast nucleation restricts the time available for the formed nanoparticles to increase their size [73]. This can result in the formation of a higher number of smaller particles in a shorter time, contrasting with lower concentrations where particles could have more time to increase their size. The increase in the polyphenol concentration increases the number of nucleation sites in the solution. Furthermore, high polyphenol concentrations behave as a stabiliser that restricts the growth of the formed nanoparticles and increases their size [73]. Based on Yuan et al. [81], the polyphenols of PPE also behave as a capping agent where they adsorb onto the surface of the nanoparticles, hindering their aggregation. These results are in good agreement with other published literature. [82–84] Therefore, it can be concluded that the PPE is largely responsible for providing high catalytic activity of the synthesised CuO-SiO_2/RGO catalyst in the transesterification and esterification reaction of WVO. To investigate further the reason for the OPA monomer yield and understand the deactivation mechanism, the fresh and spent catalysts were extensively characterised. Fig. 2(b) indicates

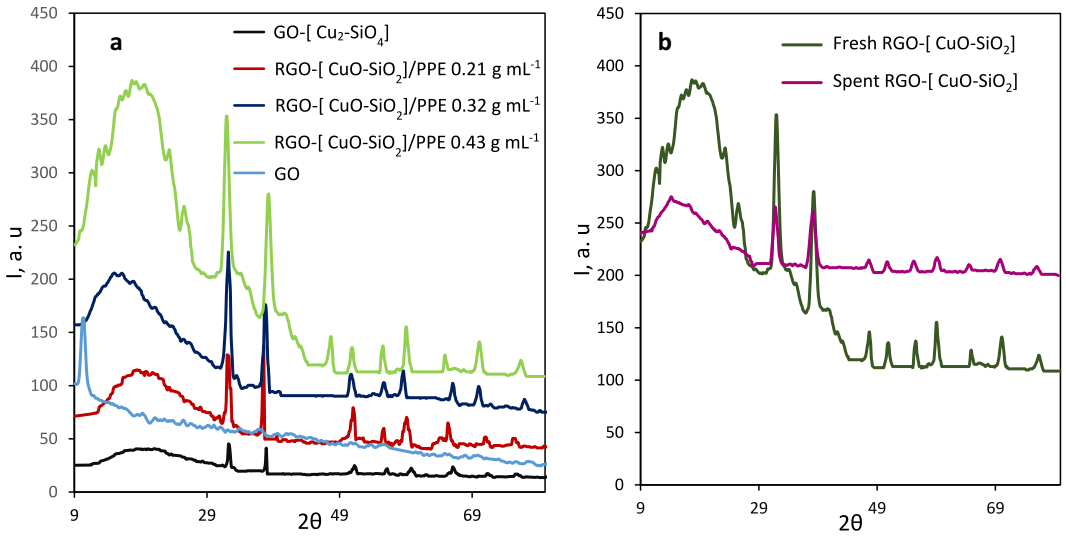

Fig. 2. XRD patterns of (a) CuO-SiO_2/RGO nanocomposite synthesised with different PPE concentrations and (b) GO, fresh and spent CuO-SiO_2/RGO nanocomposite catalyst.

the XRD pattern of fresh and spent CuO-SiO_2/RGO nanocomposite catalyst. The XRD pattern of the fresh catalyst demonstrates the presence of active complexes for the transesterification and esterification reaction, i.e. CuO and SiO_2. The literature has reported these complexes' high activity as a catalyst for both reactions, respectively [75,76]. The XRD pattern of the spent catalyst demonstrated a high resemblance to the fresh unused CuO-SiO_2/RGO nanocomposite catalyst, suggesting that it did not significantly change its chemical structure. The decreased peak intensity of the spent catalyst evidenced the coverage of its surface with WVO. These results are in agreement with the results reported by Dias et al. [85] and Deng et al. [86]

3.1.2. *FT-IR spectra of CuO-SiO_2/RGO nanocomposite catalyst*

FT-IR spectra were utilised to determine the functional groups that exist in GO, along with the nanostructures synthesised with different PPE concentrations as indicated in Fig. 3(a). FT-IR spectra of GO show an absorption band at 3440 cm^{-1}, which was attributed to the stretching vibrations of–OH. The peaks at 2930 cm^{-1} and 1050 cm^{-1} were assigned to C—H and stretching vibrations C—O [87], respectively. The FTIR spectra of the nanocomposite sample prepared with no PPE content demonstrate a high-intensity peak at 3450 cm^{-1} assigned to free O—H of GO. The FT-IR spectrum also shows characteristic peaks at 1630 cm^{-1} corresponding to (C—O) due to the incorporation of graphene sheets and the (O—H) bond of water. The characteristic peaks at 460 cm^{-1} and 1088 cm^{-1} were assigned to the stretching vibrations Si–O–Si and Si–O–Cu/Si–O–Si of amorphous SiO_2 as detected in the XRD patterns [88], respectively. The peaks at 968, and 807 cm^{-1} were also assigned to the stretching vibrations of Si–OH and Si–O–Si, respectively. The absorption peaks at 825–840 cm^{-1} are owing to the vibration of SiO_4 groups of Cu_2SiO_4. The intensity of these absorption peaks of SiO_4 significantly decreases with the increase of PPE concentration and completely diminishes when PPE concentration increases above 0.21 g mL^{-1} was applied suggesting the phase transformation of Cu_2-SiO_4 to mixed oxide CuO-SiO_2, which is evidenced by the XRD pattern of the synthesised catalyst. The FT-IR spectra demonstrate the characteristic peaks of Cu—O at 670, 570 and 430 cm^{-1}, which confirm the presence of

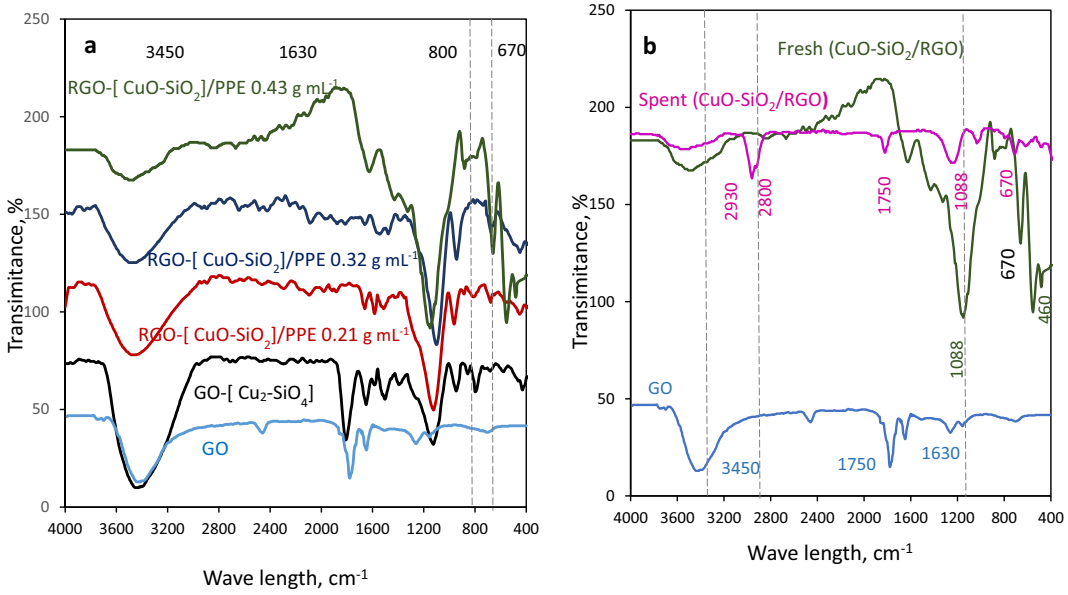

Fig. 3. FTIR characterisation of (a) CuO-SiO_2/RGO nanocomposite catalyst synthesised with different PPE concentrations, (b) GO, fresh and spent CuO-SiO_2/RGO nanocomposite catalyst.

the copper nanoparticle. The intensity of the peaks at 3450 cm^{-1}, 1744.8 cm^{-1} and 1628 cm^{-1} significantly decreased with the increase of PPE concentration, which suggests a reduction of functional groups with oxygen by PPE solution. The characteristic peaks at 1744.8 cm^{-1} and 1628 cm^{-1} correspond to C—H stretching completely and disappear at a high PPE solution concentration of 0.4 M. All the observed peaks confirm the creation of a new metal-oxygen bond of Cu—O and Si–O–Si in the structure of the catalyst, which coordinated with XRD data. The appearance of these peaks proves the successful synthesis of CuO-SiO_2/RGO nanocomposite.

Further, the FTIR spectrum was utilised to evaluate the change in the chemical structure on the catalyst surface. Fig. 3(b) demonstrates the FTIR spectra of fresh and spent CuO-SiO_2/RGO nanocomposites. The characteristic peak at 1674 cm^{-1} on the FTIR spectra of the fresh catalyst proves the adsorption of water molecules on the catalyst's surface. On the other hand, the spent CuO-SiO_2/RGO nanocomposite shows a new sharp band at 1745.10 cm^{-1} that can be attributed to the presence of carbonyl stretching vibration of triglycerides (C=O). Furthermore, the presence of absorption peaks of -CH_2- and -CH_3- of the fatty acid chain is situated at 2800 cm^{-1}, and 2930 cm^{-1}, respectively [89,90]. The presence of all these new peaks confirms the direct interactions between WVO fatty acids and the synthesised catalyst, where alkyl fatty acids cover the surface of the catalyst as indicated in the proposed reaction mechanism introduced in section 5.7. These results indicate that the

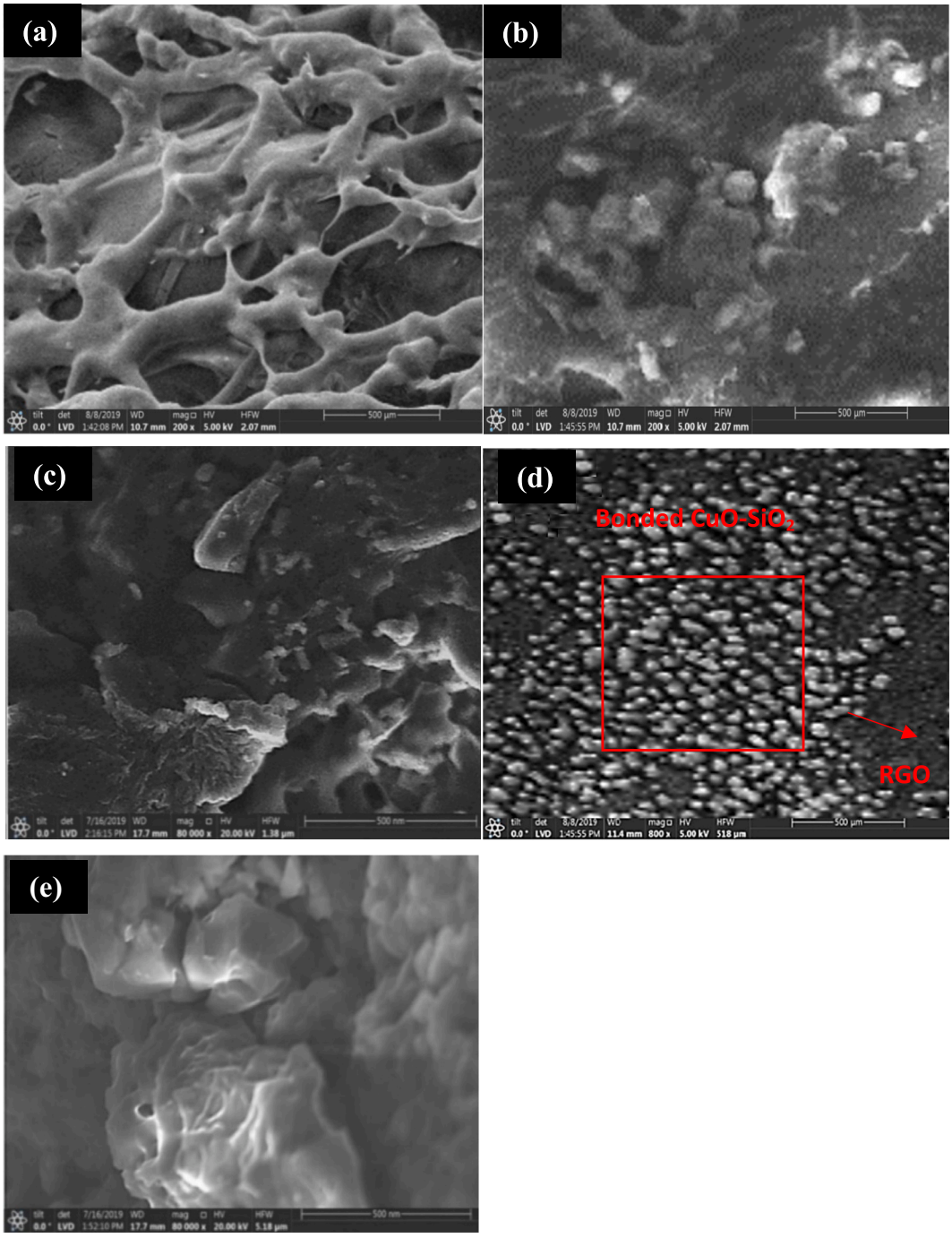

Fig. 4. SEM images of CuO-SiO_2/RGO nanocomposite catalyst synthesised with different PPE concentrations (a) GO-[Cu_2SiO_4] (no PPE content), (b) RGO-[CuO-SiO_2]/PPE 0.2 g mL^{-1}. (c) RGO-[CuO-SiO_2]/PPE 0.3 g mL^{-1} (d) RGO-[CuO-SiO_2]/PPE 0.4 g mL^{-1}(e) Spent CuO-SiO_2/RGO catalyst.

organic components of WVO cover the catalyst's surface, which influences the availability of the active sites of the catalyst.

3.1.3. Scanning electron microscope (SEM) with energy dispersive X-ray (EDX) analysis

The surface morphology of nanostructures synthesised with various concentrations of PPE solutions is indicated in Fig. 4 (a-d) for further investigation of the effect of PPE on the shape and size of the synthesised nano-catalyst.

Fig. 4(a) shows the SEM image of GO-[Cu_2SiO_4] nanostructure before the addition of PPE solution, where a clear irregular sheet-like structure with a continuous layer was observed, signifying incomplete reduction in the absence of polyphenols. As can be observed in Fig. 4(b), the incorporation of 0.21 g mL^{-1} PPE solution highly changed the surface from planar microstructures to non-uniform nano-bundles of relatively large and sparsely distributed CuO–SiO_2 particles along the RGO surface. This can be attributed to lower nucleation sites at insufficient polyphenol concentration, permitting larger particles to grow. Fig. 4(c) demonstrates less distinct nanoparticles on the RGO layer, despite a reduction in crystallite size from 26 nm to 15 nm with increasing PPE concentration from 0.21 to 0.32 g mL^{-1}, as evidenced by XRD analysis. This could be attributed to the formation of ultra-small nanoparticles (~15 nm) that are partially embedded in RGO matrix, thereby limiting the visibility of some particles in SEM imaging. The behaviour reported in other literature, where ultrafine metal oxide was difficult *to* resolve by SEM while it was proved by diffraction [91]. Fig. 4(d) shows the SEM image of the CuO-SiO_2/RGO nanocomposite catalyst synthesised by applying 0.43 g mL^{-1}, PPE solution. As indicated, a higher-density nanoparticle-like structure with localised aggregation can be observed. The XRD and TEM of the synthesised CuO-SiO_2/RGO nanocomposite using 0.43 g mL^{-1}, PPE solution confirmed that the crystallite sizes are 7 nm and 6.67 nm, respectively, suggesting that the detected localised aggregation is owing to the agglomerated ultrafine primary nanoparticles. The behaviour attributed to the high surface energy of the ultrasmall nanoparticles resulted from a higher reduction rate and an increased nucleation promoted by the abundant polyphenols [92]. Similar results have been reported in another literature where SEM results revealed larger particle size, compared to XRD and TEM, owing to particle aggregation [93]. These results confirm that the PPE concentration has a substantial influence on the nanoparticles formation and morphology. Although the increase of PPE concentration endorses smaller particles, excessive concentrations can disturb its stability, resulting in a degree of aggregation. Particle aggregation of ultrasmall oxide nanoparticles at excessively increased concentration of reducing agent has been reported previously [94,95].

The creation of uniform CuO-SiO_2 nanoparticles on RGO sheets at higher PPE concentrations can be attributed to the shielding effect of PPE solution that modifies the size and shape of the particles to a nanoscale, owing to the presence of polyphenols in PPE solution that behave as a reducing agent. Increasing the concentration of polyphenols with the increase of PPE concentration enhances the reduction reaction rate, which reduces the copper and silica ions faster which resulting in the fast nucleation of nanoparticles. The higher nucleation rate owing to a higher concentration of polyphenols acts as a reducing agent and leads to the formation of smaller nanoparticles, which can further aggregate [82–84]. Furthermore, the conception of the steric hindrance effect and capping effects of polyphenols during the synthesis of the nano-catalyst results in better control of the shape and size of the catalyst's particles. The presence of negatively charged hydroxyl groups of polyphenols in PPE results in a decrease in the size of the formed particles, as indicated in Figs. 4 (a-d), resulting in better control of particle aggregations that aid in the formation of uniform CuO-SiO_2 nanoparticles doped on RGO sheets. This was in line with the principle mentioned by Aisida et al. [73] The morphological change of the synthesised nanoparticles from irregular shape to spherical nanoparticles with the increase of reducing agent extract has also been reported in other literature [96] where polyphenols of PPE solution act as a capping and stabilising agent, which averts any further growth of nanoparticles after they are formed. The polyphenols of PPE adsorb on the surface of the produced particles, forming a hydrogen bond between these particles and the hydroxyl groups of polyphenols, which hinders particle agglomeration through the steric hindrance technique [96,97]. Therefore, these results introduce the usage of PPE as a novel and sustainable reactant that can be utilised for in situ synthesis of uniform CuO-SiO_2/RGO nanocomposite catalysts. Hence, optimising the applied PPE solution concentration is a key parameter for efficient control of the shape and size of CuO-SiO_2/RGO nanocomposite catalyst.

The SEM image of the fresh catalyst Fig. 4(d) shows a dense nanoparticle-like structure of grafted along the RGO grafted along the RGO surface can be observed, which demonstrates high catalytic activity of the catalyst. The uniform nanoparticle-like structure with spaces between the nanoparticles is a favourable catalyst morphology for the transesterification reaction [98]. After the transesterification and esterification occurred on the surface of the catalyst, the SEM image of the spent catalyst Fig. 4(e) indicates an unclear, rugged surface due to the coverage of the catalyst surface with oily fatty acids, which reinforced the previous observation by XRD and FTIR characterisation. Despite the rugged surface of the spent catalyst, the coverage of some active sites with WVO components could be a reason for the loss of catalytic activity of the catalyst. The transesterification and esterification reactions that happened on the surface of CuO-SiO_2/RGO nanocomposite are the reasons for the morphological changes reported before and after the reaction.

The comparison between the nanocomposite control sample synthesised with no PPE content and the PPE-derived nanocomposite catalyst further highlights the role of the PPE in the synthesis of the nanocomposite catalyst. The FTIR and XRD results of the prepared nanocomposite with no PPE content indicated the formation of Cu_2SiO_4 supported on GO, resulting from the interaction of Cu^{2+} and SO_3^{2-} ions in the presence of the GO solution (Fig. 2A and Fig. 3A). The morphological study of Cu_2SiO_4/GO further indicated the absence of a dispersed nanoparticle structure, demonstrating poor structural development without the application of PPE. In contrast, the presence of PPE facilitated the reduction of Cu^{2+} to CuO, condensation of silica, and a reduction of GO to RGO, resulting in the formation of uniformly dispersed CuO–SiO_2 nanoparticles on RGO sheets.

Fig. S1, supporting information, demonstrates the EDX analysis of the CuO-SiO_2/RGO nanocomposite catalyst (Fig. 5a) and spent CuO-SiO_2/RGO catalyst obtained from the reaction with WVO (Fig. 5b). These investigations yield elemental compositions of the samples that evidence the obtained results from XRD and FTIR. Fig. (5a) indicates the weight compositions of carbon, oxygen, silica, and copper are 19.43, 30.42, 19.81 and 30.34 %, respectively. In Fig. (5b), the weight compositions of carbon, oxygen, silica and copper are 37.43, 20.42, 14.81 and 27.34 %, respectively. The characterisation of the spent CuO-SiO_2/RGO demonstrates that the initial weight percent of copper and silica is reduced, whereas the weight percent of carbon increases. To explain these changes, a proposed reaction mechanism is introduced in section 3.6. The elemental composition of fresh and spent CuO-SiO_2/RGO catalyst was further evaluated by EDS mapping as indicated in Fig. 5(a)-(h), which indicates the existence of 4 elements of C, O, Cu and Si.

3.1.4. Transmission electron microscopy (TEM) analysis

The TEM image of GO in Fig. 6(a) indicates a plate/sheet-like morphology. Whereas CuO-SiO_2/RGO nanocomposite Fig. 6(b) shows a uniform distribution of spherical CuO-SiO_2 nanoparticles on the RGO sheets, which reveals the presence of a chemical bond between mixed ions and inorganic nanoparticles CuO-SiO_2 and RGO sheets, which is crucial for efficient catalytic performance. According to the TEM results, the average particle size of the synthesised catalyst is 6.72 nm, which was in good agreement with the results of XRD.

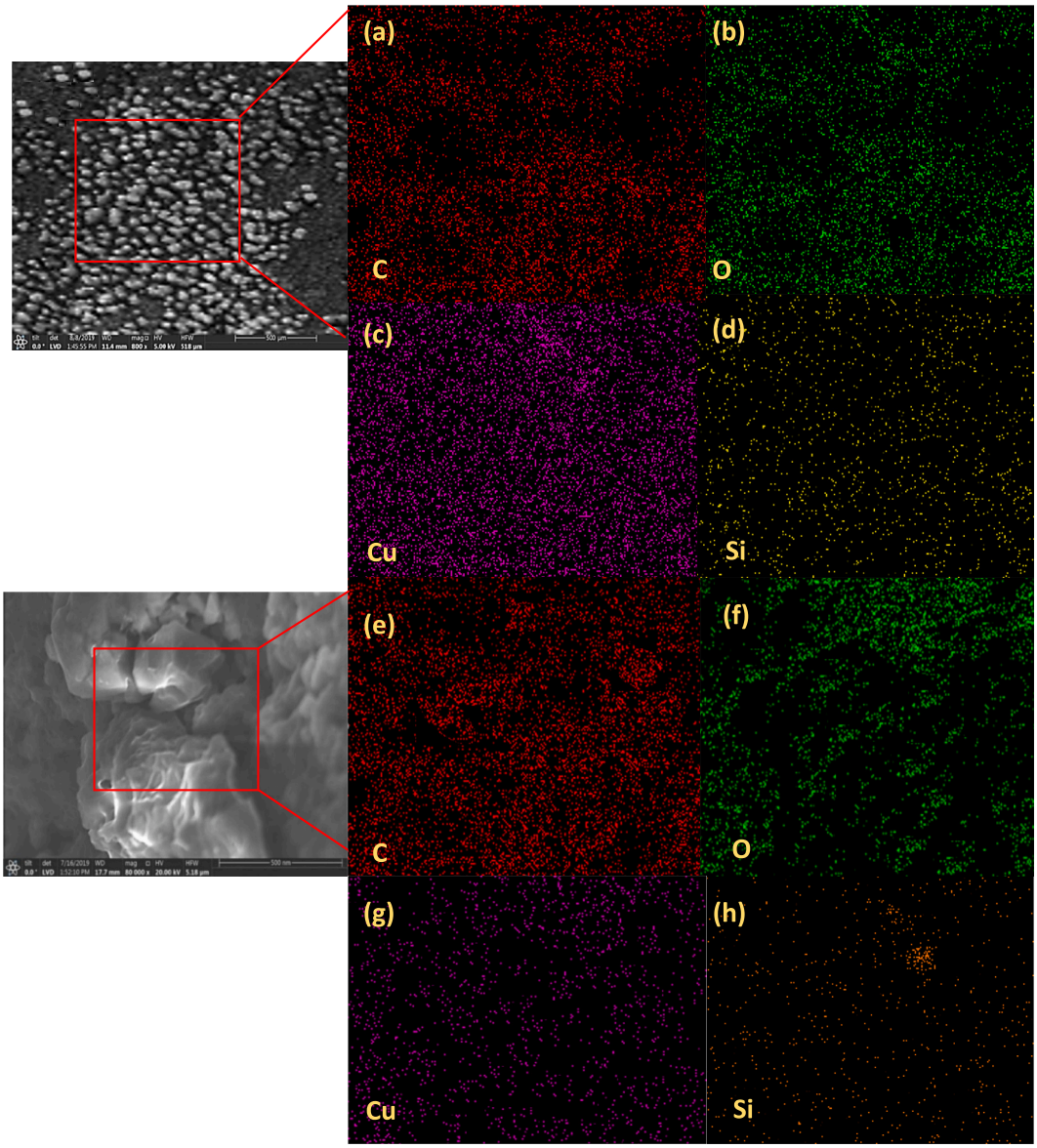

Fig. 5. SEM-EDX mapping of fresh CuO-SiO_2/RGO catalyst before the reaction (a) C; (b) O; (c) Cu; (d) Si; SEM-EDS mapping of spent CuO-SiO_2/RGO catalyst after the reaction and (e) C; (f) O; (g) Cu; (h) Si.

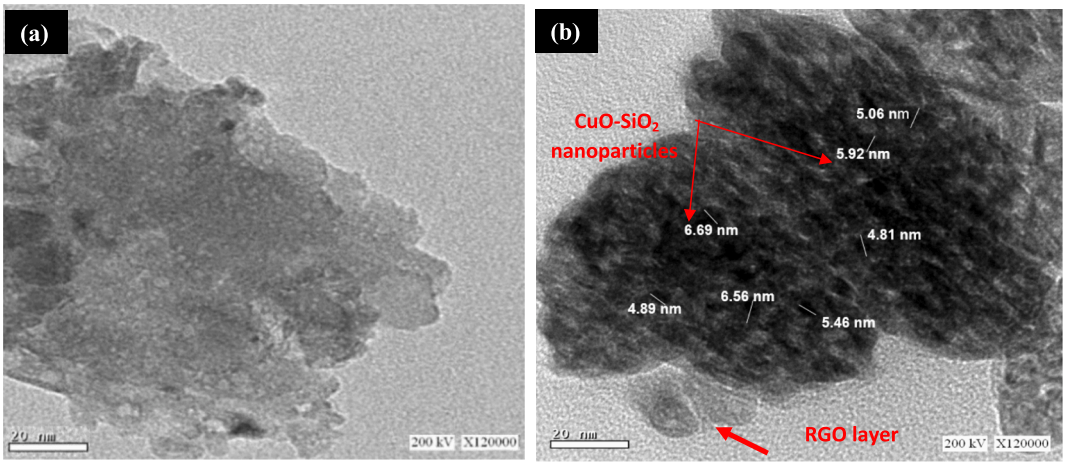

Fig. 6. TEM image of (a) GO and (b) CuO-SiO_2/RGO nanocomposite catalyst.

3.1.5. TGA/DTA analysis of synthesised CuO-SiO_2/RGO nanocomposite catalyst

Fig. 7 demonstrates the TGA and DTA curves of GO and CuO-SiO2/RGO nanocomposite catalyst. For GO, the onset degradation temperature of GO where 10 % mass loss was observed is ~180 °C. The following thermal decomposition stage was at 200–300 °C with a weight loss of ~40 %. The complete decomposition of the GO sample was reported at approximately 700 °C. The DTA curves exhibit two peaks at 230 and 630 °C. The first peak corresponds to the pyrolysis of unstable oxygen-containing functional groups that exist on the GO surface [99], while moderately stable oxygen-containing functional groups decompose at a higher temperature of 630 °C [100]. The TGA and DTA curve of CuO-SiO_2/RGO nanocomposite catalyst demonstrates higher thermal stability compared with GO, which is proved by the significant increase in T_{10} value °C to 421 °C and the considerable decrease in the peaks of the DTA curve. The obtained TGA and DTA curves of CuO-SiO_2/RGO nanocomposite catalyst demonstrate the first decomposition stage at 430 °C, which is attributed to the pyrolysis of organic components, mostly the oxygen-containing functional groups on RGO, i.e. carboxyl, hydroxyl groups that result in the release of CO, CO_2. It is worth noting that the weight loss of CuO-SiO_2/RGO nanocomposite catalyst due to the decomposition of the remaining functional group process is much less than that of the GO (10 wt%), which proves the elimination of the oxygen-containing functional groups through the reduction reaction initiated by PPE [101]. The last degradation stage started at a temperature of 538 °C, which is due to the pyrolysis of the carbon skeleton of RGO [102].

3.2. Model fitting and adequacy checking

Design Expert software developed a regression equation signifying the relationship between reaction variables and response. Accordingly, a quadratic model has been constructed to fit the actual experimental results as indicated in Eq. 11.

$$Y_1 = 84 + 14.25\,A + 9.33\,B + 14.42C + 13.00\,D + 7.75\,AB + 12.25\,AC + 9.75\,CE + 11.25\,BCE + 11.5\,BD + 11.75CD - 21.00\,A^2 - 13.37\,B^2 - 28.75\,C^2 - 24.63\,D^2 \quad (11)$$

Where Y_1 is the dependent variable of OPA monomer yield, while *A, B, C* and *D* are the independent variables; HPA: WVO molar ratio, catalyst loading, temperature, and time, respectively.

The generated model has been evaluated for adequacy to define any errors related to normal assumptions. The regression equation clarifies the influence of the reaction variables on the responses. The positive sign of each parameter signifies the synergetic influence, whereas the negative sign signifies the antagonistic influence [103]. The generated RSM model has been validated by ANOVA via evaluating the F-test and *p*-values. As indicated in Table 3, the F-test and p-values are 60.08 and < 0.0001, respectively, which proves the statistical significance of the developed quadratic models. It is also observed that the lack-of-fit value is 0.0558 (not significant), which indicates that the model represents most of the experimental data accurately. The values of the determination coefficient, $R^2$and R^2_{adj}, which assess the accuracy of the model fitting, have been reported to be 0.9836 and 0.9673, respectively. These values illustrate that around 98.3 % of the variance has been related to the variables, which proves the accuracy of the generated model to fit the experimental data.

The performance of the model has been evaluated using various methods. As indicated in Fig. S2, supporting information, the predicted versus experimental result of OPA monomer yield displayed high correlation and good agreement. The accurate estimation of the model response values is concluded from the reasonable agreement between the predicted and actual experimental results. Fig. S3, supporting information, shows a plot of residual distribution versus predicted response that has been introduced to evaluate the capability of the model to fit the experimental results. Residual value is stated as a variance between the experimental and predicted values of a defined response. The data presented in Fig. S4, supporting information, proves that the generated model adequately signifies the experimental results owing to its random distribution as a function of the predicted response values. Furthermore, the perturbation plot clarifies the influence of each variable on the response as indicated in Fig. S5, supporting information. As sharp curvature from the centre point shows the high significance of the model's variable, which proves the statistical results attained from ANOVA. As indicated in Fig. S4, supporting information, the independent variables HPA:WVO molar ratio (A), catalyst loading (B), temperature (C) and (D) time have a highly significant effect on model response (OPA yield). It also signifies the influence of each variable, as for the HPA:WVO molar ratio, the plot clarifies that it has a marked increasing influence on OPA yield until it reaches a maximum point, where it barely decreases beyond this point.

3.3. Effect of process variables

3.3.1. Effect of individual process variables

Experimental runs have been conducted at HPA:WVO molar ratios between 2:1 and 10:1 to investigate the influence of their change on the yield of the OPA monomer. According to the ANOVA results summarised in Table 3, the HPA:WVO molar ratio has a highly significant influence on the OPA yield. The HPA:WVO molar ratio displays a linear

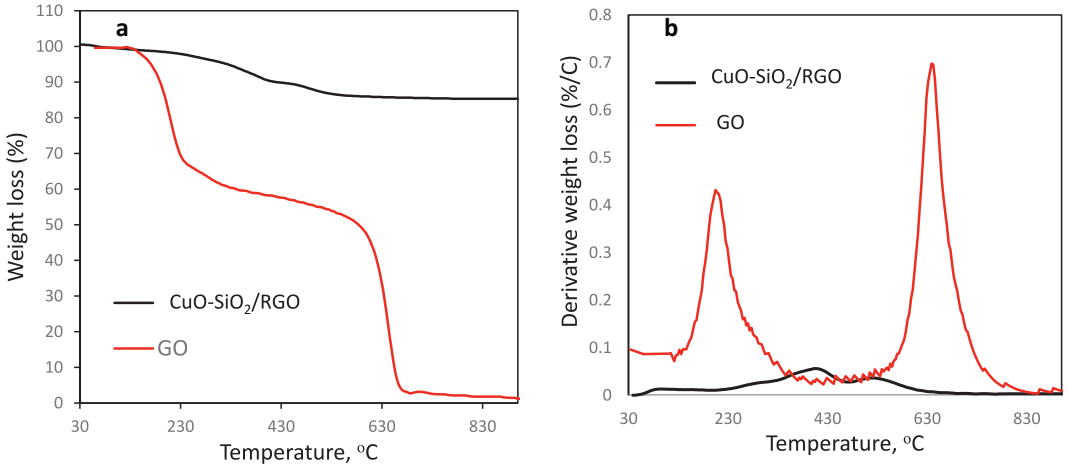

Fig. 7. (a) Thermogravimetric analysis (TGA) and (b) differential thermal analysis (DTA) of GO sheets and CuO-SiO_2/RGO nanocomposite catalyst.

relationship with the transesterification reaction catalytic performance as an ~88.9 % yield of OPA was obtained at a higher HPA:WVO molar ratio of (7.9:1). As indicated in Fig. S5, supporting information, the OPA yield increased from 53.1 % to 88.9 % as HPA:WVO molar ratio increased from 2:1 to 7.9:1. However, OPA yield significantly decreased at HPA:WVO molar ratio higher than 7.9:1. The increase of OPA yield with HPA:WVO molar ratio can be attributed to increased conversion rate of the transesterification reaction controlled by the Le Chatelier principle in the existence of high concentration of HPA in the reaction mixture [104]. Further, the decrease in OPA yield could be due to the dissolution of produced glycerol in a large amount of HPA that hinders the reaction of HPA with the catalyst and WVO, as indicated in the transesterification reaction mechanism in Fig. 10. Gendy et al. [103] reported that excessive concentration of the hydroxyl group during the transesterification reaction of WVO prevents the separation of glycerol, which drives the equilibrium back to the reactant side, hence decreasing the reaction's yield. The same observation has also been reported by Dukare et al. [105] They have reported that an excessive increase in the molar concentration of the hydroxyl group negatively affects the rate of conversion of the transesterification reaction owing to limited mass transfer.

The ANOVA results, summarised in Table 3, indicate that catalyst loading has a highly significant effect on OPA yield. It is observed in Fig. S5, supporting information, that the yield of OPA monomer increases with the increase of the catalyst loading. For the reaction conducted with 0.5 % (*w*/w) catalyst loading, the OPA yield was ~61.4 %. Whereas a further increment in the yield of OPA (~86.6 %) was noted at 2.4 % (w/w) catalyst loading. The high yield attained with the increase of catalyst loading up to 2.4 % (w/w) may be owing to the presence of a huge number of active sites that facilitate the transesterification reaction. Additionally, there was a decrease in the OPA yield as the catalyst loading increased beyond 2.4 % (w/w). This indicates that the produced active sites for the reaction between WVO and HPA were sufficient at 2.4 % (w/w) catalyst loading. Hence, increasing the catalyst loading above 2.4 % (w/w) is not required. Zubir and Chin [106] reported similar phenomena. They reported that the reaction equilibrium was reached faster at a higher concentration of catalyst loading, owing to the increase in available active sites for the reaction. The decrease of OPA yield with further increase of catalyst loading beyond 2.4 wt% can be attributed to the increase of the viscosity of the reaction mixture, which restricts the mass transfer of the WVO-HPA catalyst system.

The summarised ANOVA results in Table 3 indicate that the reaction temperature has a highly significant effect on OPA yield. It is indicated in Fig. S5 supporting information that the OPA yield increases with the increment of the reaction temperature from 25 and 92 °C. The increase of OPA yield with the reaction temperature can be attributed to the increased mass transfer at the phase interface with increasing temperature. At a lower reaction temperature, the available energy to have enough collisions between WVO and HPA with the catalyst is insufficient. However, at the higher reaction temperatures, the opportunity for collision between WVO and HPA is improved and easily attains the needed activation energy to proceed with the reaction [107]. Furthermore, the increase in temperature would improve the constant rate of transesterification and esterification reactions [103] which results in a rapid synthesis of OPA monomer. At a reaction temperature of 92 °C, the yield of OPA was~86.4 %. However, the OPA yield decreased at higher reaction temperature values (≤92 °C).

As indicated in Fig. S5 supporting information, the reaction time has almost a linear relationship with OPA yield within the range of 1 to 10.6 h; however, the OPA yield significantly decreased at a longer reaction time above 10.6 h. This decrease in the OPA yield is possible due to the equilibrium reached at the optimum reaction condition and the high possibility of reverse reaction at a longer reaction time [108]. Albishri et al. [109] reported similar phenomena at higher reaction times. They reported that excessive reaction time negatively affects the product yield resulting from a reverse reaction of transesterification, leading to a battering of esters, which may lead to a conversion of free fatty acids to soaps that adversely affect the rate of the transesterification reaction.

3.3.2. *Effect of variable interactions on the response*

RSM is utilised to evaluate the interactive effect of different parameters that influence the process. The consideration of the variable's interaction effect is crucial for the reaction optimisation process. The three-dimensional response surface plots and ANOVA results have been utilised to evaluate the interactive effect of variables. Furthermore, the effect of variable interaction has been demonstrated using three-dimensional surface and contour plots of OPA yield for the interaction of two variables. Fig. 8(a) indicates the three-dimensional graphical representation of the interactive effect of HPA:WVO molar ratio and the catalyst loading, where reaction temperature and time were constant at their central midpoint values. It is noted that the yield of OPA increases as the reactant molar ratio and catalyst loading increase. Maximum OPA yield is observed at a catalyst loading of 2.4 % (*w*/w) and reactant molar ratio of 7.8:1. However, the OPA yield declines as the reactant molar ratio and catalyst loading exceed 7.8:1 and 2.4 % (w/w), respectively.

Additionally, the interaction between the HPA:WVO molar ratio and reaction temperature has indicated a significant influence on OPA yield, as summarised in Table 3. The three-dimensional response surface plot between the HPA:WVO molar ratio and the reaction temperature is indicated in Fig. 8(b). The interaction is observed in Fig. 8(a), where the influence of reaction temperature at HPA:WVO molar ratio of 2:1 has an increasing influence on the OPA yield until nearly 88 °C, and above 88 °C, there is a decrease in the response of OPA yield with the increase of temperature. However, the influence of reaction temperature at HPA:WVO molar ratio of 10:1 is different where there is an increase in the OPA yield until 101 °C where a decline in the response is observed as the temperature increases at HPA:WVO molar ratio of 10:1. This demonstrates that the reaction temperature has a decreasing influence at higher values, however, the decreasing influence is more significant at HPA:WVO molar ratio of 2:1. Moreover, the effect of HPA:WVO molar ratio at 40 °C on the OPA yield indicates an increasing influence on OPA yield until HPA:WVO molar ratio, where a slight decline in the OPA yield with further increase in HPA:WVO molar ratio. However, the effect of the HPA:WVO molar ratio at 130 °C has an increasing influence on the OPA yield. The increase in OPA monomer yield with the increase in reaction temperature could be attributed to the increased reaction rate owing to the increase in the kinetic energy of the reactant. Although higher reaction temperature increases the reaction rate, it can also accelerate side reactions that compete with the transesterification reaction, which decreases the yield of the main product [110]. Therefore, the decrease of OPA monomer yield with an excessive increase of reaction temperature can be attributed to the occurrence of side reactions, i.e. the hydrolysis of triglycerides in the presence of water to FFAs, at a faster rate compared to the transesterification reaction, which negatively affects the OPA monomer yield. Similar results were concluded by Díaz et al. [111] Furthermore, high reaction temperature can also shift the equilibrium of the transesterification reaction, which leads to the formation of reactants instead of products. [112,113]

Moreover, the interaction between catalyst loading and reaction time on OPA yield is indicated in Fig. 9(a). Notably, reaction time has a different increasing influence at different levels of catalyst loading, whereas reaction time has a more significant increasing influence on the OPA yield at higher levels of catalyst loading. It is also notable that OPA yield decreases as the catalyst loading and reaction time exceed 3.5 % (*w*/w) and 10.6 h, respectively. The observed increase in OPA monomer yield could be owing to the increase in active sites with the increase in catalyst loading, which facilitated reactants' adsorption on the surface of the catalyst's active sites. Hence, a higher OPA monomer yield was obtained. Based on the results of ANOVA, the interaction effect between HPA:WVO molar ratio and reaction time has displayed a highly significant influence on OPA yield, as indicated in Table 3. The interaction effect is shown in Fig. 9(b), as at 1 h reaction time, the increase of the

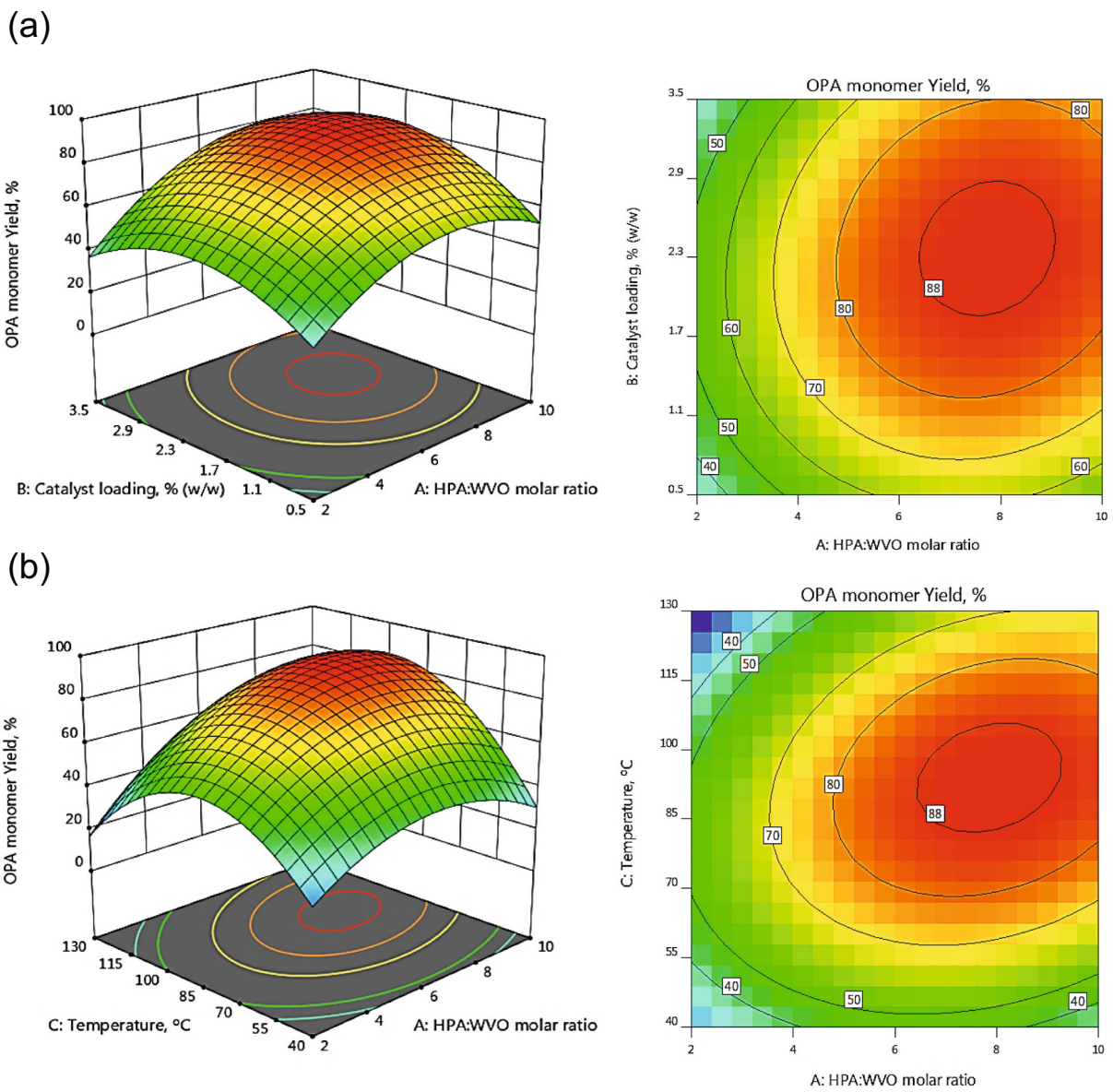

Fig. 8. Three-dimensional and contour plots for OPA monomer yield. The RSM plots were generated using the data shown in Table 2 (a) OPA monomer yield (%) as a function of HPA: WVO molar ratio and catalyst loading, and (b) OPA monomer yield (%) as a function of HPA:WVO molar ratio and temperature.

HPA:WVO molar ratio on OPA yield is approximately negligible. However, at a longer reaction time, i.e. at 15 h, the increase of HPA:WVO molar ratio has a pronounced increasing effect on the OPA yield. According to this interaction, a maximum OPA yield of about was achieved at HPA: WVO molar ratio of 7.8:1 and a reaction time of 9.4 h.

3.4. Process optimisation and experimental validation

Design Expert software was utilised to optimise the model response (OPA yield) by merging the desirability of each model variable into one value and finding the optimum value for the specified goals of the response. OPA yield has been set to the maximum target while minimising process variables as indicated in Table 4. The optimum reaction conditions have been specified via numerical optimisation at a reactant molar ratio of 8.5:1, catalyst loading of 3.5 (w/w)%, reaction temperature of 54 °C, and reaction time of 9.5 h, resulting in 95.73 % for OPA yield, respectively. The experimental validation of the optimisation results indicated an OPA yield of 96.76 %, which signifies the accuracy of the predicted optimum conditions with a 1.1 % deviation from the experimental results. To confirm the catalytic role of PPE in the synthesis of the nanocomposite, the catalytic performance of a control catalyst prepared without PPE was also assessed under the same reaction conditions. The catalytic evaluation of Cu_2SiO_4/GO control sample for the synthesis of OPA monomer was negligible of less than 10 %. Whereas CuO–SiO_2/RGO PPE-derived nanocomposite provided significantly higher OPA yield of 95.73 %. These results demonstrate the role of PPE in the formation of the active structure of the catalyst through the conversion of Cu_2SiO_4/GO intermediate product into CuO–SiO_2/RGO nanostructured composite, where polyphenols of PPE behave as green reductants, stabilising agents, and improve nucleation, resulting in a synergistic structure of CuO-SiO_2/RGO nanocomposite with high catalytic activity.

Table 5 demonstrates the comparison of the optimised synthesis conditions of OPA fatty acid monomer using the novel green CuO-SiO_2/RGO nanocomposite catalyst proposed in this research with other studies reported in the literature. The optimised OPA monomer yield attained in this research compared favourably with other reported studies, where the synthesised green CuO-SiO_2/RGO heterogeneous catalyst provided higher fatty acid monomer yield at lower reaction temperature and time compared with other heterogeneous catalysts

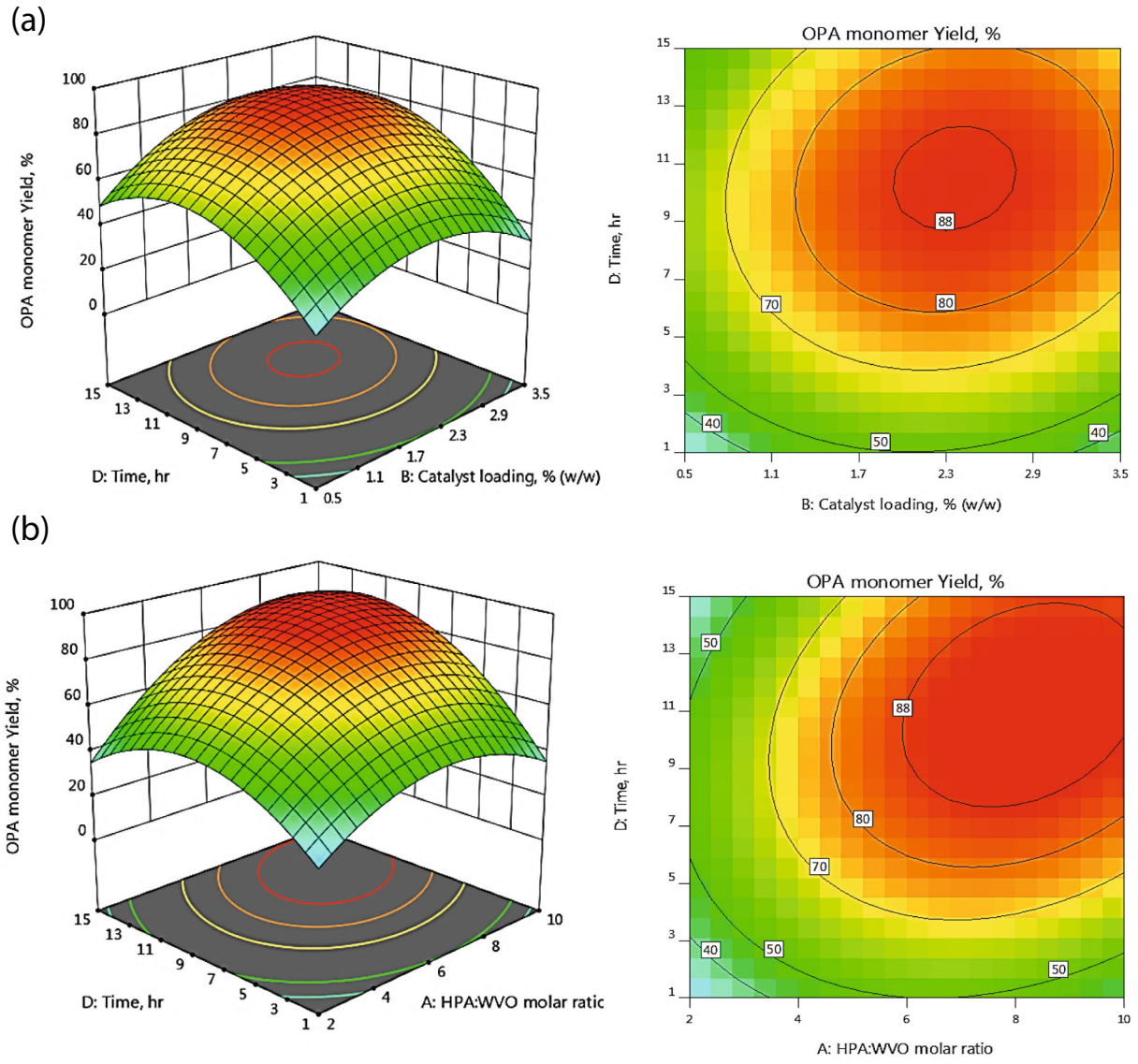

Fig. 9. Three-dimensional and contour plots for OPA monomer yield. The RSM plots were generated using the data shown in Table 2 (A) OPA monomer yield (%) as a function of catalyst loading (*w*/w) and reaction time and (B) OPA monomer yield (%) as a function of HPA:WVO molar ratio (w/w) and reaction time on OPA monomer yield.

Table 4
Optimisation constraints are used to predict the optimum composition for OPA synthesis.

Factor	Code	Goal	Importance	Limits	
			Scale 1–5	lower	upper
WVO: HPA (molar ratio)	A	Minimise	4	2	10
Catalyst loading (%) (w/w)	B	Minimise	4	0.5	3.5
Reaction temperature (°C)	C	Minimise	4	40	130
Reaction time (h)	D	Minimise	4	1	15
OPA Yield, %	Y_1	Maximise	5	80	100

reported in the literature. As indicated in Table 5, the reported heterogeneous catalysts in the literature were utilised to catalyse the esterification reaction of various fatty acids for the synthesis of fatty acid monomers, whereas the synthesised CuO-SiO_2/RGO nanocomposite catalyst reported in this research was designed to catalyse both transesterification and esterification reactions simultaneously which is the property tailored for one-pot, low-temperature synthesis of fatty acid monomer from high acid value WVO reported for the first time in this research.

3.5. Catalyst reusability study and economic assessment

The catalyst reusability study and the FTIR spectra of regenerated CuO-SiO_2/RGO catalyst are indicated in Fig. 10(a)-(b). Reusability is an imperative property of heterogeneous catalysts, as they can be recycled for further reaction with an appropriate purification process. In this research, the reusability of the CuO-SiO_2/RGO nanocomposite catalyst was examined for 5 runs. The optimum conditions of the reaction were applied to evaluate for reusability of the CuO-SiO_2/RGO catalyst for OPA synthesis. The experiments were conducted at reaction conditions of HPA:WVO 8.5, 3.5 % (*w*/w) catalyst loading, 54 °C for 9.5 h. The catalyst reusability was assessed as indicated in Fig. 10(a). The reusability of the catalyst demonstrated a maximum yield of 96.76 % ± 0.36 % in the first cycle. The used catalyst was directly reapplied to synthesise the OPA monomer at the same reaction conditions. In the second cycle, the OPA yield was almost equal to the yield obtained in the first cycle. In the third cycle, the OPA decreased to 86.3 ± 0.39 %. Further, the OPA monomer yield reached 84.6 ± 0.41 % and 76.62 ± 0.34 % after the

Table 5
Comparative study of the catalytic activity of CuO-SiO_2/RGO nanocomposite catalyst and several reported catalytic systems to synthesise fatty acid monomers.

Catalysts	Fatty acid monomer yield, %	Experimental conditions	Reaction Temperature, °C	Reaction Time, hr	Reference
Pt/Ce_2O_5	65	15 mL H_2O, pressure 34.5 atm, 1 % Pt/Ce_2O_5, Gamma valerolactone	350	10	(114)
Pd/Al_2O_3	91	Stearic acid, reaction pressure 6.91, 2 % Pd/Al_2O_3	250	24	(53)
Palladium	80	Furfural, reaction pressure 1 atm, 2 % Palladium	200	32	(115)
Pd/C	80	Stearic acid, reaction pressure 5.91 atm, Dodecane	330	6	(58, 116)
$PdCl_2$	90	Stearic acid, $PdCl_2$ (3 mol%) Ac_2O	110	18	(117, 118)
NiI_2	66	Stearic acid, NiI_2 (2.8 mol%), PPh_3 (0.14 equiv)	190	16	(119)
Chromium supported on MCM-41/O_2	32.4	Oleic acid, 2.0 MPa CO_2 followed by 1.0 MPa O_2	80	8	(120)
CuO- SiO_2/RGO	96.76	HPA:WVO 8.5, (CuO-SiO_2/RGO) 3.5 % (w/w), 90 mL of p-cymene.	54	9.5	This work

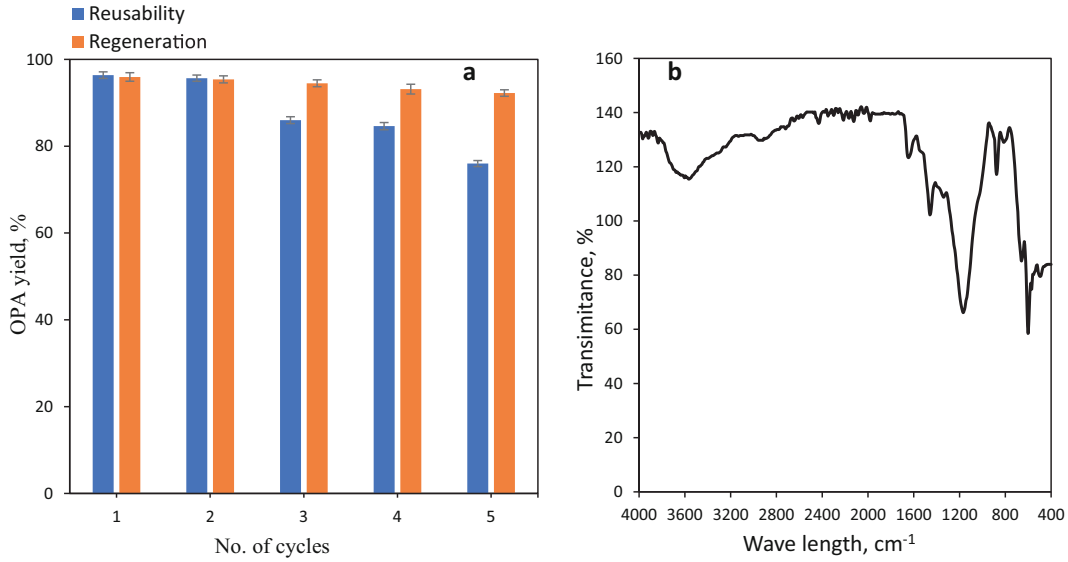

Fig. 10. (a) Catalyst reusability and regeneration studies of CuO-SiO_2/RGO on the yield of OPA. Experimental conditions: HPC:WVO molar ratio 8.5:1; catalyst loading 3.5 % (*w*/w), reaction temperature 54 °C and reaction time 9.5 h. (b) FTIR of calcinated CuO-SiO_2/RGO nanocomposite catalyst.

fourth and fifth cycles, respectively. The aforementioned results suggested that the stability of the catalyst gradually decreased after the second cycle of reusability. As evidenced from the XRD, FTIR, SEM and EDX analysis of the fresh and spent CuO-SiO_2/RGO nanocomposite catalyst, the transesterification and esterification occurred on the surface of the catalyst, resulting in the accumulation of oily molecules of WVO and the coverage of active sites of the synthesised catalyst upon usage in reusability cycles. The behaviour which hindered the catalyst's interaction with HPA monomer resulted in a decrease in the catalytic activity of the synthesised catalyst after the second cycle.

Subsequently, the CuO-SiO_2/RGO catalyst was washed with methanol and exposed to thermal treatment to remove the accumulated organic components of glycerol and residual WVO covering the catalyst's active sites and retaining the catalytic performance of the catalyst. As indicated in Fig. 10(a), the regenerated catalyst demonstrated higher OPA yield reaching 94.5 ± 0.39 %, 93.4 ± 0.51 % and 93.1 ± 0.37 % for the third, fourth and fifth cycles, respectively, with insignificant decreases in OPA yield from the first cycle. Hence, the catalyst was effectively activated after washing and calcination, demonstrating high catalytic stability up to the fifth cycle with an insignificant decrease in OPA yield. The FTIR spectra of the regenerated catalyst in Fig. 10(b) demonstrate the presence of characteristic peaks of the fresh catalyst. Furthermore, the disappearance of the characteristic peaks of fatty acid alkyl groups with calcination suggests the decomposition of fatty acid alkyl groups during the regeneration process, which enhances the surface of the catalyst and restores its catalytic activity.

Besides the catalytic performance, a preliminary cost estimate was conducted using the CatCost spreadsheet to evaluate the economic feasibility of the synthesised CuO-SiO_2/RGO nanocomposite catalyst, applying a bottom-up cost modelling approach for material, utility, and labour costs. The methodology and assumptions of the CatCost methods were previously detailed in previous publications [121]. The materials quantities from the experimental procedure and their corresponding cost were input, and the estimated cost of the synthesised CuO-SiO_2/RGO catalyst on a laboratory scale is $0.51 per gram. Given the reusability of the catalyst over 5 cycles, the effective cost per cycle is approximately $0.1 per gram. The upscaled cost for a production capacity of 1000 kg per year, including utilities and labour, is approximately $100 per kilogram. In comparison, commercial CuO or SiO_2 catalyst is priced $5–40 per gram, and Pd/C costs $33–80 per gram from typical chemical suppliers. Therefore, the proposed route provided a cost-effective solution considering the valorisation of waste PPE as a zero-cost reducing agent and the catalyst reusability up to 5 cycles at mild reaction conditions.

Furthermore, the economic viability of the synthesised OPA monomer was evaluated. Considering the zero-cost WVO, the low cost of the HPA monomer and high OPA yield under mild conditions, the calculated cost of OPA monomer in lab scale is below $200 per kilogram. The estimated cost is significantly lower than the price of long-chain fatty acid commercial analogues, priced up to $1700/kg. This emphasises the

sustainable and economic route of both the recyclable green catalyst and the fatty acid-rich monomer.

3.6. Spectroscopic analysis of OPA monomer

FT-IR spectra of WVO and the OPA thermo-sensitive monomer were evaluated to identify their feature groups (Fig. S6, supporting information). The FT-IR spectra of WVO demonstrated a peak at 3007.40 cm^{-1} that is attributed to the C—H isolated double bond. The peak at 3470 cm^{-1} corresponds to the O—H group. The peaks at 2854.42 cm^{-1}, and 2924.10 cm^{-1} are assigned to C—H of the saturated carbon chain [122]. The weak absorption peak at 967 cm^{-1} corresponds to C—H of unsaturated free fatty acids. The FT-IR spectrum of the OPA thermo-sensitive monomer demonstrated a peak at 1560 cm^{-1} corresponding to the C═C stretching vibration of the vinyl group. The band at 1630 cm^{-1} was owing to the carbonyl group, whereas peaks at 1745 cm^{-1} were assigned to the C—O ester group, which proves the incorporation of ester and vinyl groups into the fatty acid chains. The existence of a strong band at 1745 cm^{-1} shreds of evidence of the ester property of the OPA fatty acid monomer. The ^{1}H NMR spectra of the OPA monomer (Fig. S7, supporting information) show a band at $\delta = 0.87$ ppm corresponding to the terminal CH_3 group of the fatty acid chain. The band at $\delta = 2.3$ ppm is assigned to CH_2 attached to the new carbonyl group formed owing to transesterification and esterification reactions. The peak at $\delta = 1.6$ ppm is from the protons of the CH_2 group that follow it. The band at $\delta = 1.26$ ppm is from -CH_2- groups protons in the fatty acid chains. The signals at $\delta = 5.3$ ppm are attributed to protons of the -CH=CH- group. Moreover, the bands between $\delta = 5.6$–6.8 ppm are assigned to the protons of the -CH=CH_2 group. The peak at $\delta = 5$ ppm signifies the proton connected to (CH_2 = CH-C(O)). The purity of the synthesised OPA monomer was evaluated using ^{1}H NMR spectroscopy through the evaluation of the integration ratios of characteristic signals. The absence of signals of unreacted 2-hydroxy-3-phenoxypropyl acrylate, WVO, or side products proves the high purity of the synthesised OPA monomer. The estimated chemical purity of the OPA monomer is 98.86 %, which confirms the selectivity of the synthesised CuO-SiO_2/RGO catalyst and the effectiveness of the one-pot reaction.

TGA and DTA analyses have been performed for the synthesised OPA monomer to demonstrate the weight loss and mass derivative of the synthesised OPA monomer as a function of temperature. The TGA analysis (Fig. S8, supporting information) indicates a single-stage weight loss in the temperature range of 260–460 °C with approximately 3 % mass residual. The decomposition within 315 to 460 °C demonstrates the pyrolysis of hydrophobic fatty acid chains, besides the breaking of C—H and C—C bonds. From DTA curves, notably, the OPA monomer shows a single peak that corresponds to the maximum rate of

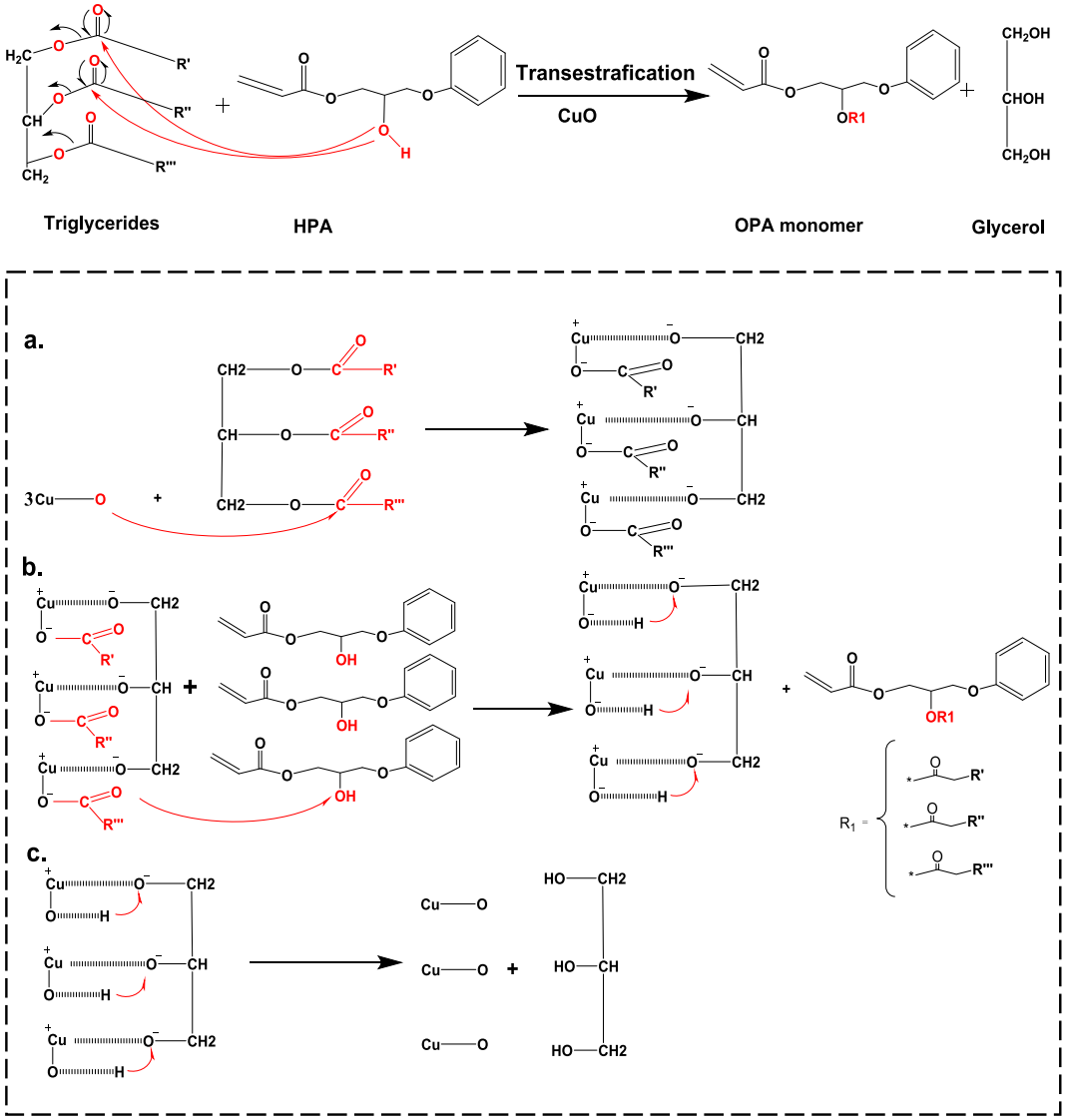

Fig. 11. Transesterification reaction mechanism of WVO triglycerides with HPA.

degradation at 384 °C. This can be attributed to the absence of free fatty acids and improved conversion to ester groups. The presence of a single degradation peak proves the uniform and slow rate of thermal decomposition at a higher temperature [123].

3.7. Plausible reaction mechanism and green metrics study for the synthesis of OPA fatty acid monomer

The plausible reaction mechanism throughout the transesterification and esterification reaction processes, for the synthesis of OPA fatty acid monomer, was proposed in view of the performed characterisation analysis of the fresh and spent CuO-SiO_2/RGO nanocomposite catalyst. The proposed transesterification and esterification reactions mechanism of HPA with WVO triglycerides and free fatty acids, respectively, is demonstrated in Figs. 11 and 12. Both transesterification and esterification simultaneously occurred on the surface of the catalysts CuO and SiO_2. According to the characterisation of the spent catalyst, the catalyst surface was shielded by the triglyceride of WVO; therefore, as indicated in Fig. 11, the CuO catalyst interacts with the triglycerides of WVO. The interaction between the CuO and triglyceride creates a bond between Cu and -O-CH_2. Hence, the FTIR spectra of the spent catalyst demonstrate an adsorption peak at 1745.1 cm^{-1} that proves the presence of the -CH_2 aliphatic group (Fig. 3). This aliphatic was reported elsewhere [89,90]. Furthermore, the FTIR spectra demonstrate the presence of the carbonyl function of the triglycerides of WVO. As indicated in Fig. 11, the interaction between CuO and triglyceride created a bond of Cu and–O-CH_2 (step A). The presence of an excess concentration of HPA monomers in the transesterification reaction eased the breakage of the interaction, as demonstrated in step B. Therefore, in step B, $H_2C{=}CHCO_2CH_2CH(O)CH_2OC_6H_5$ in the HPA replaced the O of the catalyst to get the OPA monomer. Hence, the OPA monomer was separated from the surface. Further, the residual interaction of Cu with CH_2 aliphatic was added with a hydrogen atom, creating glycerol as demonstrated in step C. Further, the glycerol was separated from the catalyst surface. On the other hand, SiO_2 worked to esterify FFA as indicated in Fig. 12 (step A). The hydrogen atom exists in FFA and RCOO- and interacts with the silica and oxygen atoms of the catalyst. The hydroxyl group of HPA can replace oxygen in SiO_2 to form H_2O, which is then separated from the catalyst as demonstrated in step B. Further, the RCOO-segment bonded with oxygen to get the OPA monomer as demonstrated in step C. The results obtained in the mechanism are in good agreement with other published literature [124].

The main aim of green chemistry is to efficiently utilise raw materials, valorise waste, and minimise the use of toxic reagents and solvents during chemical synthesis [125,126]. Various green chemistry metrics, such as the Environmental Factor (*E*-factor), Process Mass Intensity (PMI), and Atom Utilisation (AU), were evaluated in the reaction of WVO with HPA using a CuO-SiO_2/RGO nanocomposite. The E factor is defined as a ratio of the total mass of waste generated during the synthesis to the mass of the synthesised product [127,128]. The high amount of waste produced during the chemical reaction increases the value of the E-factor, which results in negative consequences on the environment. The ideal value of the *E*-factor is in the range of 0–1. During the synthesis of OPA fatty acid monomer, glycerol is produced as a byproduct, which could be further utilised in many chemical syntheses; however, it was considered as a waste that is typically produced in each cycle. The E-factor for OPA fatty acid monomer synthesis using CuO-SiO_2/RGO catalyst was evaluated at each catalyst run. As indicated in Table 6, E-factors from the 1st to 4th cycle were reported as low values that range from 0.063 to 0.037, which indicates that the synthesis process is environmentally friendly. In the 5th cycle E-factor value increased to 0.805 (less than 1) owing to the addition of the mass of

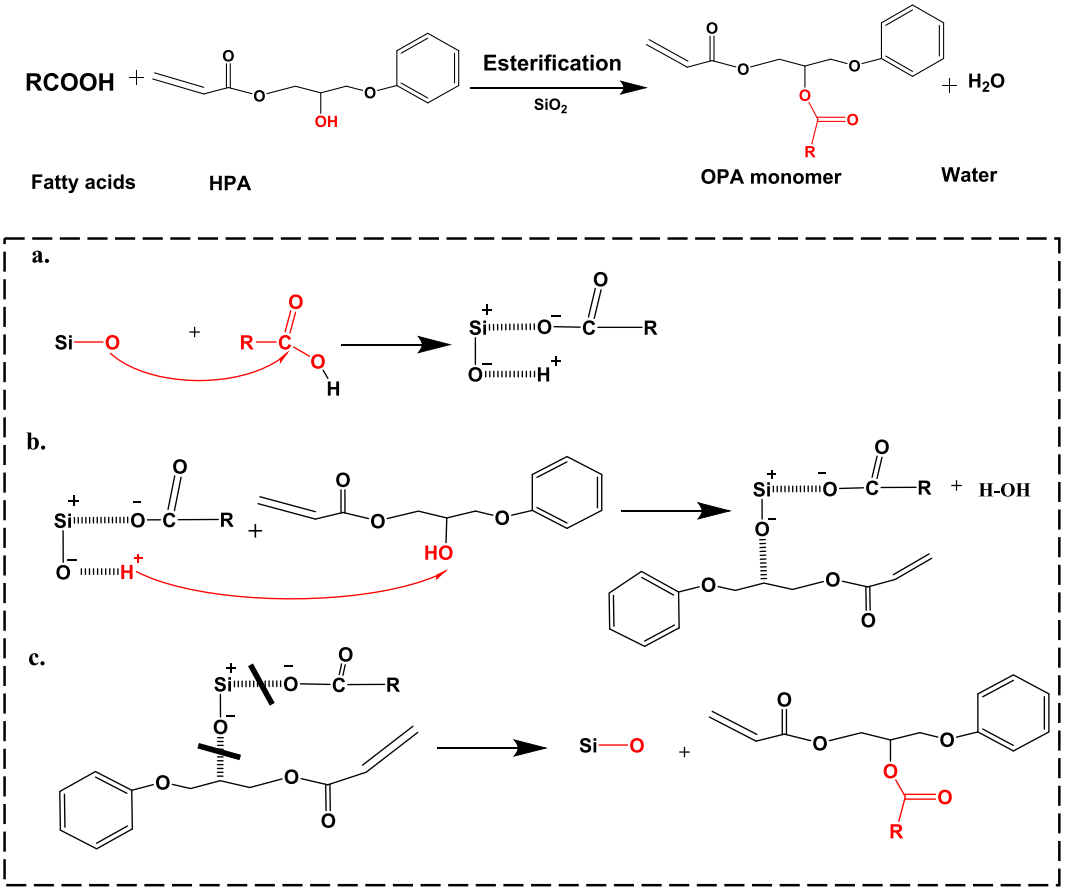

Fig. 12. Esterification reaction mechanism of free fatty acids of WVO and HPA.

Table 6
Green metrics parameter calculated for each catalyst cycle.

Parameter	1st Cycle	2nd Cycle	3rd Cycle	4th Cycle	5th Cycle
E-factor	0.0631	0.053	0.0434	0.0377	0.805
PMI	1.814	1.830	1.8480	1.875	1.893
AU	94.061	94.943	95.830	96.361	97.52
Yield %	96.250	95.40	94.50	93.150	92.25

solvent that was previously reused, which proved that the catalyst can be expressed as environmentally benign. The calculated E-factor value at each catalyst run is indicated in Table 6.

Process Mass Intensity (PMI) is another sustainability metric applied to evaluate the sustainability of a chemical reaction, which is a ratio between the mass of total mass of the reaction process to the mass of the isolated product [129,130]. Considering the mass of the reactants, solvent, catalyst, and by-products, and the main product OPA monomer, the calculated PMI values evaluated at each catalyst run as reported in Table 6 ranged from 1.81 to 1.89, which implies that CuO-SiO_2/RGO catalyst is efficient to synthesise OPA fatty acid monomer from high acid value WVO up to five cycles without triggering any environmental concerns. Correspondingly, atom utilisation (AU) is another green metric utilised to evaluate the sustainability of a chemical reaction and is concluded to be a sustainable reaction in nature. AU is defined as a ratio between the mass of the main product to the mass of all products resulting from the chemical reaction [127]. It is considered a simple and fast evaluation of the greenness of a chemical synthesis process in terms of the amount of waste produced. During the synthesis of OPA fatty acid monomer, glycerol and water are produced as by-products. Using the mass of the produced OPA fatty acid monomer, glycerol and water at each cycle, the AU value was calculated as indicated in Table 6.

4. Conclusions

The synthesised green, cost-effective CuO-SiO_2/RGO nanocomposite heterogeneous catalyst derived from the waste pomegranate peels demonstrated excellent results when applied for the synthesis of the fatty acid-rich OPA monomer from high acid value WVO. A quadratic model was developed, signifying the OPA monomer yield as a function of four reaction variables. The model predicted the optimum OPA yield of 95.73 % at HPC:WVO molar ratio of 8.5:1, catalyst loading of 3.5 % (*w*/w), reaction temperature of 54 °C, and 9.5 h reaction time. The reusability study demonstrated a decrease in OPA yield after the second run due to the coverage of the active sites of the catalyst with by-products and WVO. The catalyst regeneration by washing with methanol, followed by calcination, efficiently regenerated the catalytic activity of the synthesised catalyst. This study demonstrates, for the first time, the direct and simultaneous transesterification and esterification of high acid value WVO into an OPA monomer using a novel CuO–SiO_2 nanocomposite catalyst supported on RGO sheets. The successful utilisation of waste vegetable oil and a green, heterogeneous catalyst not only valorises low-cost waste feedstock but also paves the way for the sustainable production of fatty acid-based monomers. By integrating RSM optimisation, this research offers an innovative, cleaner, and economically viable route for synthesising fatty acid-rich monomers with wide-ranging industrial applications. These findings open new avenues for advancing circular economy approaches within the oleochemical and polymer industries.

CRediT authorship contribution statement

Shahenda Mahran: Writing – original draft, Visualization, Validation, Software, Methodology, Investigation, Formal analysis, Data curation, Conceptualization. **Maria Centeno:** Supervision. **Attia Attia:** Supervision, Resources, Project administration, Funding acquisition, Conceptualization. **Basudeb Saha:** Writing – review & editing, Visualization, Supervision, Resources, Project administration, Funding acquisition, Formal analysis, Conceptualization.

Declaration of competing interest

The authors declare that they have no known competing financial interests or personal relationships that could have appeared to influence the work reported in this paper.

Acknowledgement

The authors acknowledge The British University in Egypt (BUE) and London South Bank University (LSBU) for their support of this research. The first author also wishes to thank our former research group members, Dr. Victor Onyenkeadi and Dr. Omar Aboelazayem, for their valuable discussions and insights that contributed to this work.

Appendix A. Supplementary data

Supplementary data to this article can be found online at https://doi.org/10.1016/j.fuproc.2025.108314.

Data availability

Data will be made available on request.

References

[1] S. Mahran, A. Attia, B. Saha, Synthesis of green thermo-responsive amphoteric terpolymer functionalized silica nanocomposite derived from waste vegetable oil triglycerides for enhanced oil recovery (EOR), J. Clean. Prod. 380 (2022) 135024.
[2] K. Sharma, S.S. Toor, J. Brandão, T.H. Pedersen, L.A. Rosendahl, Optimized conversion of waste cooking oil into ecofriendly bio-based polymeric surfactant-A solution for enhanced oil recovery and green fuel compatibility, J. Clean. Prod. 294 (2021) 126214.
[3] A. Mannu, S. Garroni, J. Ibanez Porras, A. Mele, Available technologies and materials for waste cooking oil recycling, Processes 8 (3) (2020) 366.
[4] A. El-Hoshoudy, S. Desouky, A. Attia, Synthesis of starch functionalized sulfonic acid co-imidazolium/silica composite for improving oil recovery through chemical flooding technologies, Int. J. Biol. Macromol. 118 (2018) 1614–1626.
[5] S.M. Elsaeed, E.G. Zaki, W.A. Omar, A. Soliman, A.M. Attia, Guar gum-based hydrogels as potent green polymers for enhanced oil recovery in high-salinity reservoirs, ACS Omega 6 (36) (2021) 23421–23431.
[6] A.A. Soliman, A.N. El-Hoshoudy, A.M. Attia, Assessment of xanthan gum and xanthan-g-silica derivatives as chemical flooding agents and rock wettability modifiers, Oil Gas Sci. Technol. 75 (2020) 12.
[7] S. Mahran, A. Attia, B. Saha, A review on polymer flooding in enhanced oil recovery under harsh conditions, in: 11th International Sustainable Energy & Environmental Protection Conference, 2018.
[8] G.E. Azmi, A.M. Saada, E.M. Shokir, M.S. El-Deab, A.M. Attia, W.A. Omar, Adsorption of the xanthan gum polymer and sodium dodecylbenzenesulfonate surfactant in sandstone reservoirs: experimental and density function theory studies, ACS omega 7 (42) (2022) 37237–37247.
[9] H. Aboelkhair, P. Diaz, A. Attia, Biosurfactant production using Egyptian oil fields indigenous bacteria for microbial enhanced oil recovery, J. Pet. Sci. Eng. 208 (2022) 109601.
[10] H. Aboelkhair, P. Diaz, A. Attia, Environmental comparative study of biosurfactants production and optimization using bacterial strains isolated from Egyptian oil fields, J. Pet. Sci. Eng. 216 (2022) 110796.
[11] S. Mahran, A. Attia, Z. Zadeh, B. Saha, Synthesis and characterization of a novel amphoteric terpolymer nanocomposite for enhanced oil recovery applications, in: ECOS2019–32nd International Conference on Efficiency, Cost, Optimisation, Simulation and Environmental Impact on Energy Systems, 2019.
[12] M. Moreno, J.I. Miranda, M. Goikoetxea, M.J. Barandiaran, Sustainable polymer latexes based on linoleic acid for coatings applications, Prog. Org. Coat. 77 (11) (2014) 1709–1714.
[13] A. Noreen, S. Mahmood, A. Khalid, S. Takriff, M. Anjum, L. Riaz, et al., Synthesis and characterization of bio-based UV curable polyurethane coatings from algal biomass residue, Biomass Convers. Biorefinery 14 (10) (2024) 11505–11521.
[14] L. Yuan, Z. Wang, N.M. Trenor, C. Tang, Robust amidation transformation of plant oils into fatty derivatives for sustainable monomers and polymers, Macromolecules 48 (5) (2015) 1320–1328.
[15] M.M. Aung, Z. Yaakob, S. Kamarudin, L.C. Abdullah, Synthesis and characterization of Jatropha (Jatropha curcas L.) oil-based polyurethane wood adhesive, Ind. Crop. Prod. 60 (2014) 177–185.

[16] J. Hulsbosch, L. Claes, D. Jonckheere, D. Mestach, D.E. De Vos, Synthesis and characterisation of alkyd resins with glutamic acid-based monomers, RSC Adv. 8 (15) (2018) 8220–8227.

[17] R. Saada, O. AboElazayem, S. Kellici, T. Heil, D. Morgan, G.I. Lampronti, Greener synthesis of dimethyl carbonate using a novel tin-zirconia/graphene nanocomposite catalyst, Appl. Catal. B Environ. 226 (2018) 451–462.

[18] P.P. Pescarmona, M. Taherimehr, Challenges in the catalytic synthesis of cyclic and polymeric carbonates from epoxides and CO_2, Cat. Sci. Technol. 2 (11) (2012) 2169–2187.

[19] E. Başţürk, M.V. Kahraman, Photocrosslinked biobased phase change material for thermal energy storage, J. Appl. Polym. Sci. 133 (32) (2016).

[20] N. Mhadeshwar, K. Wazarkar, A.S. Sabnis, Synthesis and characterization of ricinoleic acid derived monomer and its application in aqueous emulsion and paints thereof, Pigm. Resin Technol. 48 (1) (2019) 65–72.

[21] T.O. Machado, P.B. Cardoso, P.E. Feuser, C. Sayer, P.H. Araújo, Thiol-ene miniemulsion polymerization of a biobased monomer for biomedical applications, Colloids Surf. B: Biointerfaces 159 (2017) 509–517.

[22] M. Piccini, D.J. Leak, C.J. Chuck, A. Buchard, Polymers from sugars and unsaturated fatty acids: ADMET polymerisation of monomers derived from D-xylose, D-mannose and castor oil, Polym. Chem. 11 (15) (2020) 2681–2691.

[23] P.A. Fokou, M.A. Meier, Use of a renewable and degradable monomer to study the temperature-dependent olefin isomerization during ADMET polymerizations, J. Am. Chem. Soc. 131 (5) (2009) 1664–1665.

[24] P.K. Dannecker, U. Biermann, A. Sink, F.R. Bloesser, J.O. Metzger, M.A. Meier, Fatty acid–derived aliphatic long chain polyethers by a combination of catalytic ester reduction and ADMET or thiol-ene polymerization, Macromol. Chem. Phys. 220 (4) (2019) 1800440.

[25] L.M. Lillie, W.B. Tolman, T.M. Reineke, Structure/property relationships in copolymers comprising renewable isosorbide, glucarodilactone, and 2, 5-bis (hydroxymethyl) furan subunits, Polym. Chem. 8 (24) (2017) 3746–3754.

[26] K. Nomura, P. Chaijaroen, M.M. Abdellatif, Synthesis of biobased long-chain polyesters by acyclic diene metathesis polymerization and tandem hydrogenation and depolymerization with ethylene, ACS omega 5 (29) (2020) 18301–18312.

[27] D. Le, C. Samart, S. Kongparakul, K. Nomura, Synthesis of new polyesters by acyclic diene metathesis polymerization of bio-based α, ω-dienes prepared from eugenol and castor oil (undecenoate), RSC Adv. 9 (18) (2019) 10245–10252.

[28] S.C. Cermak, T.A. Isbell, Synthesis and physical properties of cuphea-oleic estolides and esters, J. Am. Oil Chem. Soc. 81 (3) (2004) 297–303.

[29] S.C. Cermak, T.A. Isbell, Physical properties of saturated estolides and their 2-ethylhexyl esters, Ind. Crop. Prod. 16 (2) (2002) 119–127.

[30] T.A. Isbell, M.R. Edgcomb, B.A. Lowery, Physical properties of estolides and their ester derivatives, Ind. Crop. Prod. 13 (1) (2001) 11–20.

[31] T.A. Isbell, Chemistry and physical properties of estolides, Grasas Aceites 62 (1) (2011) 8–20.

[32] A.I. Adeleye, S. Kellici, T. Heil, D. Morgan, M. Saha Vickers, B., Greener synthesis of propylene carbonate using graphene-inorganic nanocomposite catalysts, Catal. Today 256 (2015) 347–357.

[33] M.J. Borah, A. Devi, R.A. Saikia, D. Deka, Biodiesel production from waste cooking oil catalyzed by in-situ decorated TiO_2 on reduced graphene oxide nanocomposite, Energy 158 (2018) 881–889.

[34] A.S. Yusuff, A.O. Gbadamosi, L.T. Popoola, Biodiesel production from transesterified waste cooking oil by zinc-modified anthill catalyst: parametric optimization and biodiesel properties improvement, J. Environ. Chem. Eng. 9 (2) (2021) 104955.

[35] N.S. Kolhe, A.R. Gupta, V.K. Rathod, Production and purification of biodiesel produced from used frying oil using hydrodynamic cavitation, Resour.-Effic. Technol. 3 (2) (2017) 198–203.

[36] S.K. Bhatia, R. Gurav, T.-R. Choi, H.J. Kim, S.-Y. Yang, H.-S. Song, Conversion of waste cooking oil into biodiesel using heterogenous catalyst derived from cork biochar, Bioresour. Technol. 302 (2020) 122872.

[37] X. Peng, Y. Yang, J. Wang, W. Yuan, Y. Guo, W. Hu, Cu/Fe co-modified nitrogen self-doped biochar as a heterogeneous Fenton-like catalyst for degradation of organic pollutants: Synthesis, performance, and mechanistic study, J. Environ. Chem. Eng. 11 (5) (2023) 110866.

[38] T.A.F. De Carvalho, G. Brenord, B.F. Pinto, M.K. de Albuquerque Mendes, D.S. N. Silva, AdAL e Silva, Lindgrenite as an efficient heterogeneous catalyst to obtain biodiesel, J. Environ. Chem. Eng. 12 (1) (2024) 111672.

[39] M. Janković, S. Sinadinović-Fišer, O. Govedarica, J. Pavličević, J. Budinski-Simendić, Kinetics of soybean oil epoxidation with peracetic acid formed in situ in the presence of an ion exchange resin: pseudo-homogeneous model, Chem. Ind. Chem. Eng. Q. 23 (1) (2017) 97–111.

[40] G. Sudha, H. Kalita, S. Mohanty, S.K. Nayak, Castor oil modified by epoxidation, transesterification, and acrylation processes: Spectroscopic characteristics, Int. J. Polym. Anal. Charact. 22 (6) (2017) 519–525.

[41] E. Dehonor marquez, Jf. Nieto alarcon, E. Vigueras santiago, S. Hernandez Lopez, Effective and Fast Epoxidation Reaction of Linseed Oil Using 50 wt% Hydrogen Peroxyde, 2018.

[42] T.D. Zeleke, Y.M. Ayana, Epoxidation of vernonia oil in acidic ion exchange resin, Am. J. Appl. Chem. 5 (1) (2017) 1–6.

[43] P.T. Wai, P. Jiang, Y. Shen, P. Zhang, Q. Gu, Y. Leng, Catalytic developments in the epoxidation of vegetable oils and the analysis methods of epoxidized products, RSC Adv. 9 (65) (2019) 38119–38136.

[44] R. Turco, C. Pischetola, M. Di Serio, R. Vitiello, R. Tesser, E. Santacesaria, Selective epoxidation of soybean oil in the presence of h–y zeolite, Ind. Eng. Chem. Res. 56 (28) (2017) 7930–7936.

[45] M.-Y. Yao, Y.-B. Huang, X. Niu, H. Pan, Highly efficient silica-supported peroxycarboxylic acid for the epoxidation of unsaturated fatty acid methyl esters and vegetable oils, ACS Sustain. Chem. Eng. 4 (7) (2016) 3840–3849.

[46] S. Dworakowska, C. Tiozzo, M. Niemczyk-Wrzeszcz, P. Michorczyk, N. Ravasio, R. Psaro, Mesoporous molecular sieves containing niobium (V) as catalysts for the epoxidation of fatty acid methyl esters and rapeseed oil, J. Clean. Prod. 166 (2017) 901–909.

[47] B. Nim, P. Sreearunothai, A. Petchsuk, P. Opaprakasit, Preparation of TiO_2-loaded electrospun fibers of polylactide/poly (vinylpyrrolidone) blends for use as catalysts in epoxidation of unsaturated oils, J. Nanopart. Res. 20 (2018) 1–15.

[48] S. Phimsen, H. Yamada, T. Tagawa, W. Kiatkittipong, K. Kiatkittipong, N. Laosiripojana, Epoxidation of methyl oleate in a TiO_2 coated-wall capillary microreactor, Chem. Eng. J. 314 (2017) 594–599.

[49] M. Moreno, M. Goikoetxea, J.C. de la Cal, M.J. Barandiaran, From fatty acid and lactone biobased monomers toward fully renewable polymer latexes, J. Polym. Sci. A Polym. Chem. 52 (24) (2014) 3543–3549.

[50] P. Eor, N. Tryon-Tasson, S. Kong, E.A. Smith, J.L. Anderson, Deconvoluting the combined effects of gas composition and temperature on olefin selectivity for separations using silver (I) ions in ionic liquids, ACS Meas. Sci. Au 3 (1) (2022) 53–61.

[51] R. Gosselink, W. Xia, M. Muhler, K. De Jong, J. Bitter, Enhancing the activity of Pd on carbon nanofibers for deoxygenation of amphiphilic fatty acid molecules through support polarity, ACS Catal. 3 (10) (2013) 2397–2402.

[52] E. Ochoa, W. Henao, S. Fuertes, D. Torres, T. Van Haasterecht, E. Scott, Synthesis and characterization of a supported Pd complex on carbon nanofibers for the selective decarbonylation of stearic acid to 1-heptadecene: the importance of subnanometric Pd dispersion, Cat. Sci. Technol. 10 (9) (2020) 2970–2985.

[53] J. Howeizi, S. Taghvaei-Ganjali, M. Malekzadeh, F. Motiee, S. Sahebdelfar, Effect of preparation parameters on properties and performance of Pd/Al_2O_3 catalyst in saturation of olefins, Res. Chem. Intermed. 45 (2019) 3165–3181.

[54] O. Satoshi, W. Markus, M. Kozo, Y. Jun, Mechanism of olefin hydrogenation catalysis driven by palladium-dissolved hydrogen, J. Phys. Chem. 120 (2016) 11481.

[55] T. Pan, J. Deng, Q. Xu, Y. Zuo, Q.X. Guo, Y. Fu, Catalytic conversion of furfural into a 2, 5-furandicarboxylic acid-based polyester with total carbon utilization, ChemSusChem 6 (1) (2013) 47–50.

[56] A. Chatterjee, V.R. Jensen, A heterogeneous catalyst for the transformation of fatty acids to α-olefins, ACS Catal. 7 (4) (2017) 2543–2547.

[57] G.J.S. Dawes, E.L. Scott, J. Le Nôtre, J.P. Sanders, J.H. Bitter, Deoxygenation of biobased molecules by decarboxylation and decarbonylation–a review on the role of heterogeneous, homogeneous and bio-catalysis, Green Chem. 17 (6) (2015) 3231–3250.

[58] J.P. Ford, J.G. Immer, H.H. Lamb, Palladium catalysts for fatty acid deoxygenation: influence of the support and fatty acid chain length on decarboxylation kinetics, Top. Catal. 55 (2012) 175–184.

[59] A. Chatterjee, S.H.H. Eliasson, V.R. Jensen, Selective production of linear α-olefins via catalytic deoxygenation of fatty acids and derivatives, Catal. Sci. Technol. 8 (6) (2018) 1487–1499.

[60] T. Ismail, P. Sestili, S. Akhtar, Pomegranate peel and fruit extracts: a review of potential anti-inflammatory and anti-infective effects, J. Ethnopharmacol. 143 (2) (2012) 397–405.

[61] H.N. Rajha, T. Mhanna, S. El Kantar, A. El Khoury, N. Louka, R.G. Maroun, Innovative process of polyphenol recovery from pomegranate peels by combining green deep eutectic solvents and a new infrared technology, Lwt 111 (2019) 138–146.

[62] M.R. Bertolo, V.C. Martins, M.M. Horn, L.B. Brenelli, A.M. Plepis, Rheological and antioxidant properties of chitosan/gelatin-based materials functionalized by pomegranate peel extract, Carbohydr. Polym. 228 (2020) 115386.

[63] Z. Derakhshan, M. Ferrante, M. Tadi, F. Ansari, A. Heydari, M.S. Hosseini, Antioxidant activity and total phenolic content of ethanolic extract of pomegranate peels, juice and seeds, Food Chem. Toxicol. 114 (2018) 108–111.

[64] T.P. Magangana, N.P. Makunga, O.A. Fawole, U.L. Opara, Processing factors affecting the phytochemical and nutritional properties of pomegranate (Punica granatum L.) peel waste: A review, Molecules 25 (20) (2020) 4690.

[65] Mh. Bouricha, R. Hammoudi, M. Rouibah, S. Khenfer, S.B. Bouafia, H. Benlkhelfa, et al., Biosynthesis of cupric oxide nanoparticles derived from pomegranate peel extract: A sustainable approach with antioxidant, antimicrobial, and photocatalytic capabilities, Inorg. Chem. Commun. 168 (2024) 112862.

[66] W. Abdussalam-Mohammed, M. Khlifa, A.M. Aljarani, A. Farj, M.A. Alwahsh, Biocompatible Copper Oxide Nanoparticles Functionalized by Aqueous Pomegranate Peel Extract: Characterization and Their Antibacterial Activities, 2025.

[67] H. Sun, Y. Liu, Y. Zhou, Z. Chen, J. Li, Green synthesis of iron-based nanoparticles using pomegranate leaf extracts: characterization, biomolecules and indole removal, Water 16 (18) (2024) 2665.

[68] M.S. Alhumaimess, A.A. Essawy, M.M. Kamel, I.H. Alsohaimi, H.M. Hassan, Biogenic-mediated synthesis of mesoporous Cu2O/CuO nano-architectures of superior catalytic reductive towards nitroaromatics, Nanomaterials 10 (4) (2020) 781.

[69] M. Orrico, G. Pota, V. Venezia, B. de Gennaro, G. Landi, F. Tescione, et al., Phenolic driven decoration of silica with Ag nanoparticles: Towards sustainable water remediation, J Water Process Eng 59 (2024) 105079.

[70] F.B. Moussa, H. Meskher, S. Menaa, F. Bencheikh, F.Z. Nouasria, A. Henni, et al., Dual green reduction mechanisms to prepare rGO-CoNPs nanocomposite using pomegranate peel extract: Electrochemical and photocatalysis applications, Chem. Phys. Lett. 851 (2024) 141490.

[71] A.P. Devi, D.K. Padhi, A. Madhual, P.M. Mishra, A.K. Behera, Plant biomass driven synthesis of gAu/RGO nanocomposite towards photocatalytic degradation of phenolic compounds in wastewater, J. Environ. Chem. Eng. 11 (3) (2023) 110161.
[72] O. Aboelazayem, N.S. El-Gendy, A.A. Abdel-Rehim, F. Ashour, M.A. Sadek, Biodiesel production from castor oil in Egypt: Process optimisation, kinetic study, diesel engine performance and exhaust emissions analysis, Energy 157 (2018) 843–852.
[73] M. Srivastava, A.K. Das, P. Khanra, M.E. Uddin, N.H. Kim, J.H. Lee, Characterizations of in situ grown ceria nanoparticles on reduced graphene oxide as a catalyst for the electrooxidation of hydrazine, J Mater Chem A 1 (34) (2013) 9792–9801.
[74] W.S. Hummers Jr., R.E. Offeman, Preparation of graphitic oxide, J. Am. Chem. Soc. 80 (6) (1958) 1339.
[75] M.K. Yadav, A.V. Kothari, D.G. Naik, V.K. Gupta, Morphological silica-supported acid catalyst for esterification of aliphatic fatty acid, Green Chem. Lett. Rev. 2 (3) (2009) 181–187.
[76] A. Aziz, M. Ahmad, M. Zafar, A.-R.Z. Gaafar, M.S. Hodhod, S. Sultana, Novel copper oxide phyto-nanocatalyst utilized for the synthesis of sustainable biodiesel from citrullus colocynthis seed oil, Processes 11 (6) (2023) 1857.
[77] Z. Demchuk, O. Shevchuk, I. Tarnavchyk, V. Kirianchuk, A. Kohut, S. Voronov, Free radical polymerization behavior of the vinyl monomers from plant oil triglycerides, ACS Sustain. Chem. Eng. 4 (12) (2016) 6974–6980.
[78] J. Yuan, J. Huang, G. Wu, J. Tong, G. Xie, J.-a. Duan, Multiple responses optimization of ultrasonic-assisted extraction by response surface methodology (RSM) for rapid analysis of bioactive compounds in the flower head of Chrysanthemum morifolium Ramat, Ind. Crop. Prod. 74 (2015) 192–199.
[79] B. Li, H. Cao, ZnO@ graphene composite with enhanced performance for the removal of dye from water, J. Mater. Chem. 21 (10) (2011) 3346–3349.
[80] P. Fakhri, B. Jaleh, M. Nasrollahzadeh, Synthesis and characterization of copper nanoparticles supported on reduced graphene oxide as a highly active and recyclable catalyst for the synthesis of formamides and primary amines, J. Mol. Catal. A Chem. 383 (2014) 17–22.
[81] M. Jiménez-Rosado, A. Gomez-Zavaglia, A. Guerrero, A. Romero, Green synthesis of ZnO nanoparticles using polyphenol extracts from pepper waste (Capsicum annuum), J. Clean. Prod. 350 (2022) 131541.
[82] A. Salayová, Z. Bedlovičová, N. Daneu, M. Baláž, Z. Lukáčová Bujňáková, Ľ. Balážová, Green synthesis of silver nanoparticles with antibacterial activity using various medicinal plant extracts: Morphology and antibacterial efficacy, Nanomaterials 11 (4) (2021) 1005.
[83] S.O. Aisida, K. Ugwu, P.A. Akpa, A.C. Nwanya, P.M. Ejikeme, S. Botha, Morphological, optical and antibacterial study of green synthesized silver nanoparticles via Vernonia amygdalina, Mater Today Proc 36 (2021) 199–203.
[84] F. Erci, R. Cakir-Koc, I. Isildak, Green synthesis of silver nanoparticles using Thymbra spicata L. var. spicata (zahter) aqueous leaf extract and evaluation of their morphology-dependent antibacterial and cytotoxic activity, Artif. Cells Nanomed. Biotechnol. 46 (sup1) (2018) 150–158.
[85] A.P. Soares Dias, J. Bernardo, P. Felizardo, M.J. Neiva Correia, Biodiesel production by soybean oil methanolysis over SrO/MgO catalysts the relevance of the catalyst granulometry, Fuel Process. Technol. 102 (2012) 146–155.
[86] X. Deng, Z. Fang, Y.-h. Liu, C.-L. Yu, Production of biodiesel from Jatropha oil catalyzed by nanosized solid basic catalyst, Energy 36 (2) (2011) 777–784.
[87] J. Fu, M. Zhang, L. Jin, L. Liu, N. Li, L. Shang, Enhancing interfacial properties of carbon fibers reinforced epoxy composites via Layer-by-Layer self assembly GO/SiO2 multilayers films on carbon fibers surface, Appl. Surf. Sci. 470 (2019) 543–554.
[88] G. Wu, L. Ma, L. Liu, L. Chen, Y. Huang, Preparation of SiO2–GO hybrid nanoparticles and the thermal properties of methylphenylsilicone resins/SiO2–GO nanocomposites, Thermochim. Acta 613 (2015) 77–86.
[89] H. Quan, Z. Li, Z. Huang, Self-assembly properties of a temperature-and salt-tolerant amphoteric hydrophobically associating polyacrylamide, RSC Adv. 6 (54) (2016) 49281–49288.
[90] J. Wu, H.-F. Wang, X.-B. Wang, H.-Y. Yang, R.-Y. Jiang, R.J. Zeng, Design and characterization of a microbial self-healing gel for enhanced oil recovery, RSC Adv. 7 (5) (2017) 2578–2586.
[91] E.C. Alegria, A.P. Ribeiro, M. Mendes, A.M. Ferraria, AmBd. Rego, A.J. Pombeiro, Effect of phenolic compounds on the synthesis of gold nanoparticles and its catalytic activity in the reduction of nitro compounds, Nanomaterials 8 (5) (2018) 320.
[92] L. Wu, W. Wen, X. Wang, D. Huang, J. Cao, X. Qi, et al., Ultrasmall iron oxide nanoparticles cause significant toxicity by specifically inducing acute oxidative stress to multiple organs, Part. Fibre Toxicol. 19 (1) (2022) 24.
[93] L.A. Raj, R. Pavithra, S.K.R. Namasivayam, Green route synthesis of highly stable zinc oxide nanoparticles using root extract of andrographis paniculata and evaluation of their potential activities, Plant Nano Biol 12 (2025) 100162.
[94] S. Tang, X. Yang, C. Wang, C. Wang, Effects of polyphenols on the structure, interfacial properties, and emulsion stability of pea protein: different polyphenol structures and concentrations, Molecules 30 (8) (2025) 1674.
[95] S. Xu, X. Bai, J. Ma, M. Xu, G. Hu, T.D. James, et al., Ultrasmall organic nanoparticles with aggregation-induced emission and enhanced quantum yield for fluorescence cell imaging, Anal. Chem. 88 (15) (2016) 7853–7857.
[96] M.A.T. Safa, H. Koohestani, Green synthesis of silver nanoparticles with green tea extract from silver recycling of radiographic films, Results Eng. 21 (2024) 101808.
[97] C. Vanlalveni, S. Lallianrawna, A. Biswas, M. Selvaraj, B. Changmai, S.L. Rokhum, Green synthesis of silver nanoparticles using plant extracts and their antimicrobial activities: A review of recent literature, RSC Adv. 11 (5) (2021) 2804–2837.
[98] M.B. Gawande, A. Goswami, F.-X. Felpin, T. Asefa, X. Huang, R. Silva, Cu and Cu-based nanoparticles: synthesis and applications in catalysis, Chem. Rev. 116 (6) (2016) 3722–3811.
[99] M.-J. Hwang, M.-G. Kim, S. Kim, Y.C. Kim, H.W. Seo, J.K. Cho, Cathodic electrophoretic deposition (EPD) of phenylenediamine-modified graphene oxide (GO) for anti-corrosion protection of metal surfaces, Carbon 142 (2019) 68–77.
[100] A.G. Bannov, M.V. Popov, P.B. Kurmashov, Thermal analysis of carbon nanomaterials: advantages and problems of interpretation, J. Therm. Anal. Calorim. 142 (1) (2020) 349–370.
[101] P. Song, X. Zhang, M. Sun, X. Cui, Y. Lin, Synthesis of graphene nanosheets via oxalic acid-induced chemical reduction of exfoliated graphite oxide, RSC Adv. 2 (3) (2012) 1168–1173.
[102] R. Sarkar, S. Gajurel, A. Gupta, Pal Kumar, A., Synergistic catalysis by copper oxide/graphene oxide nanocomposites: a facile approach to prepare quinazolines and quinazoline containing triazole/tetrazole moieties under mild reaction conditions, ChemistrySelect 7 (22) (2022) e202200297.
[103] N.S. El-Gendy, A. El-Gharabawy, S. Amr, F.H. Ashour, Response surface optimization of an alkaline transesterification of waste cooking oil, Int. J. ChemTech Res. 8 (8) (2015) 385–398.
[104] M. Kadi, N. Akkouche, S. Awad, K. Loubar, M. Tazerout, Kinetic study of transesterification using particle swarm optimization method, Heliyon 5 (8) (2019) e02146.
[105] M.B. Dukare, D.S. Awasthi, D.V. Sapkal, D.R. Sapkal, Two step process for biodiesel production using non-edible oils, Indian Chem. Eng. 52 (3) (2010) 254–262.
[106] M. Zubir, S. Chin, Kinetics of modified zirconia-catalyzed heterogeneous esterification reaction for biodiesel production, J. Appl. Sci. 10 (21) (2010) 2584–2589.
[107] M.I. Al-Widyan, A.O. Al-Shyoukh, Experimental evaluation of the transesterification of waste palm oil into biodiesel, Bioresour. Technol. 85 (3) (2002) 253–256.
[108] T. Wei, M. Wang, W. Wei, Y. Sun, B. Zhong, Effect of base strength and basicity on catalytic behavior of solid bases for synthesis of dimethyl carbonate from propylene carbonate and methanol, Fuel Process. Technol. 83 (1–3) (2003) 175–182.
[109] H.M. Albishri, O.A. Almaghrabi, T.A. Moussa, Characterization and chemical composition of fatty acids content of watermelon and muskmelon cultivars in Saudi Arabia using gas chromatography/mass spectroscopy, Pharmacogn. Mag. 9 (33) (2013) 58.
[110] V. Veljković, S. Lakićević, O. Stamenković, Z. Todorović, M. Lazić, Biodiesel production from tobacco (Nicotiana tabacum L.) seed oil with a high content of free fatty acids, Fuel 85 (17–18) (2006) 2671–2675.
[111] G.C. Díaz, NdlCO Tapanes, L.D.T. Câmara, D.A. Aranda, Glycerol conversion in the experimental study of catalytic hydrolysis of triglycerides for fatty acids production using Ni or Pd on Al_2O_3 or SiO_2, Renew. Energy 64 (2014) 113–122.
[112] N.R. Ravuru, D. Rathore, Y. Agrawal, Production of biodiesel by transesterification: a green approach to energy, Interactions 245 (1) (2024) 118.
[113] M. Berrios, M. Martín, A. Chica, A. Martín, Study of esterification and transesterification in biodiesel production from used frying oils in a closed system, Chem. Eng. J. 160 (2) (2010) 473–479.
[114] J.C. Serrano-Ruiz, D. Wang, J.A. Dumesic, Catalytic upgrading of levulinic acid to 5-nonanone, Green Chem. 12 (4) (2010) 574–577.
[115] L.J. Gooßen, N. Rodríguez, A mild and efficient protocol for the conversion of carboxylic acids to olefins by a catalytic decarbonylative elimination reaction, Chem. Commun. 6 (2004) 724–725.
[116] J.W. Baek, Y.B. Hyun, H.J. Lee, J.C. Lee, S.M. Bae, Y.H. Seo, Selective trimerization of α-Olefins with immobilized chromium catalyst for lubricant base oils, Catalysts 10 (9) (2020) 990.
[117] S.H.H. Eliasson, A. Chatterjee, G. Occhipinti, V.R. Jensen, Green solvent for the synthesis of linear α-olefins from fatty acids: ACS sustain, Chem. Eng. 7 (2019) 4903–4911.
[118] D.E. Jose, U. Kanchana, T.V. Mathew, Recent developments of supported Palladium nanocatalyst and magnetically separable supported Palladium nanocatalysts for Heck cross-coupling reactions, J. Nanopart. Res. 24 (5) (2022) 89.
[119] X. Miao, C. Fischmeister, P.H. Dixneuf, C. Bruneau, J.-L. Dubois, J.-L. Couturier, Polyamide precursors from renewable 10-undecenenitrile and methyl acrylate via olefin cross-metathesis, Green Chem. 14 (8) (2012) 2179–2183.
[120] S.E. Dapurkar, H. Kawanami, T. Yokoyama, Y. Ikushima, Catalytic oxidation of oleic acid in supercritical carbon dioxide media with molecular oxygen, Top. Catal. 52 (2009) 707–713.
[121] K.M. Van Allsburg, E.C. Tan, J.D. Super, J.A. Schaidle, F.G. Baddour, Early-stage evaluation of catalyst manufacturing cost and environmental impact using CatCost, Nat. Catal. 5 (4) (2022) 342–353.
[122] R. Naveenkumar, G. Baskar, Process optimization, green chemistry balance and technoeconomic analysis of biodiesel production from castor oil using heterogeneous nanocatalyst, Bioresour. Technol. 320 (2021) 124347.
[123] M.E. Brown, Introduction to Thermal Analysis: Techniques and Applications, Springer, 2001.
[124] G. Pradhan, Y.C. Sharma, A greener and cheaper approach towards synthesis of glycerol carbonate from bio waste glycerol using CaO–TiO2 Nanocatalysts, J. Clean. Prod. 315 (2021) 127860.

[125] S. Ahmadzadeh, M. Dolatabadi, In situ generation of hydroxyl radical for efficient degradation of 2, 4-dichlorophenol from aqueous solutions, Environ. Monit. Assess. 190 (2018) 1–11.
[126] M. Dolatabadi, M. Mehrabpour, M. Esfandyari, S. Ahmadzadeh, Adsorption of tetracycline antibiotic onto modified zeolite: Experimental investigation and modeling, MethodsX 7 (2020) 100885.
[127] M. Tobiszewski, M. Marć, A. Gałuszka, J. Namieśnik, Green chemistry metrics with special reference to green analytical chemistry, Molecules 20 (6) (2015) 10928–10946.
[128] R.A. Sheldon, The E factor 25 years on: the rise of green chemistry and sustainability, Green Chem. 19 (1) (2017) 18–43.
[129] K. Budzinski, M. Blewis, P. Dahlin, D. D'Aquila, J. Esparza, J. Gavin, Introduction of a process mass intensity metric for biologics, New Biotechnol. 49 (2019) 37–42.
[130] E.R. Monteith, P. Mampuys, L. Summerton, J.H. Clark, B.U. Maes, C.R. McElroy, Why we might be misusing process mass intensity (PMI) and a methodology to apply it effectively as a discovery level metric, Green Chem. 22 (1) (2020) 123–135.

Basudeb **Saha** is the Group Lead and Director of Studies for Chemical Engineering and an Associate Director of the Centre for Global Eco-Innovation at Lancaster University, UK. He is an Honorary Professor at the University of Brunel, London and an External Examiner for the Chemical Engineering Undergraduate and Master's courses at Swansea University, UK and the University of Bradford, UK.

Before joining Lancaster University, he worked as a Professor of Chemical and Process Engineering at LSBU, UK, for over 10 years. He held various leadership roles, including Head of the Centre for Energy and the Environment Research, Founding Director of the Centre for Green Process Engineering, and Research Lead of the Applied Sciences Department at LSBU. Previously, he worked in the Chemical Engineering department of Loughborough University, UK (as a Lecturer/Senior Lecturer/Reader in Chemical Engineering) for about 14 years.

He was awarded a prestigious Royal Academy of Engineering Industrial Secondment with Syngenta Ltd. in Huddersfield, UK. He won a prestigious "Royal Society Brian Mercer Award" for developing an innovative epoxidation process technology. He is recognised as a leading expert in his field and has held Visiting Professorships at the University of Barcelona, Spain; Saga University, Japan; University of Burgos, Spain and an Adjunct Professorship at UCSI University, Malaysia. He maintains active research collaborations with The British University in Egypt, Cairo University and Port Said University.

His research focuses on innovative, greener and sustainable processes and renewable and sustainable energy solutions for which he has established an international reputation. His research team aims to tackle the climate change challenge and contribute to the net-zero emission target. His prolific contributions to the field include over 215 research papers, 7 book chapters, 1 authored/edited book, and co-inventorship of 7 patents [*h-index* of 41, with ~5800 citations (Google Scholar)]. He is currently an Editorial Board Member of *Green Processing and Synthesis Journal*, *Energies Journal*, and *Reactions Journal*; Advisory Board Member of *Reaction Chemistry and Engineering Journal*, and Editorial Board Member of *Theoretical Foundations of Chemical Engineering Journal*.

He has delivered about 100 invited and keynote lectures at national and international conferences, the House of Commons (UK Parliament), universities, research institutes, and industry. He has been invited as a member of the International Advisory and Scientific Committees of international conferences, Session Chair at national and international conferences, and a research grant reviewer of national and international funding bodies. He has co-organised sessions at national and international research events, conferences, and symposia, such as IEX 2024: Ion exchange for a sustainable future, Cambridge University, UK; Global Research Conference on Catalysis and Chemical Engineering Technology (CATCHEM2024), Munich, Germany; World Conference on Carbon 2023, Mexico; World Congress of Chemical Engineering, Barcelona, Spain etc. He has received many national and international awards (e.g. from The Royal Society, The Royal Academy of Engineering, British Council, IChemE, NRI Welfare Society, etc.) in recognition of his research excellence and scholarly achievements in Chemical Engineering.